Laser and Particle Beams (1994), *vol.* 12, *no.* 1, *pp.* 23-54
Printed in the United States of America

LISP: Laser impulse space propulsion

By C.R. PHIPPS* AND M.M. MICHAELIS†
*Los Alamos National Laboratory, Mail Stop E543, Los Alamos, NM 87545
†University of Natal, Faculty of Science, Department of Physics,
King George V Avenue, Durban 4001, South Africa

(Received 30 April 1993; revised 26 July 1993; accepted 25 September 1993)

It is not often that a new form of transportation suddenly appears and replaces what was hitherto regarded as mankind's only realistic option. In space and upper atmosphere transportation, chemical rockets have held center stage for over half a century. Tsiokolvsky's ideas led to Wernher von Braun's V2, which in turn led to the Soyuz, Apollo, and Ariane programs and the Space Shuttle. But recently theoretical and computational studies as well as a few initial experiments have pointed to a new option: laser impulse space propulsion (LISP). This may offer a more efficient and less ecologically damaging means of putting payloads into orbit. The world high-power laser community is well suited to following and aiding developments in LISP, though most practical research is still at an embryonic level. Obviously an effort of the size required to develop a laser-driven low-earth-orbit (LEO) launcher would require a multinational commitment. LISP could then be regarded as a parallel challenge to those of achieving ICF microfusion yield and of improving X-ray lasers, especially in the "water window." Any physicist or engineer involved with the latter projects would find many points in common with the former. It therefore seems appropriate to briefly review the progress made in LISP and also to communicate some recent results from high-power laser-matter experiments that have lead to conceptual designs.

1. History of laser propulsion and prospects

As early as 1956, authors were considering ground-based photonic propulsion of space vehicles (Sänger 1956). One of the earliest publications (Marx 1966) considered propulsion to relativistic velocities and first introduced the photoablation efficiency η that appears in equation (7) of this article. In the mid-1970s, a series of papers considered laser space propulsion [see Moeckel (1972a, 1972b, 1975) and Kantrowitz (1972)]. Both Sänger (1956) and Moeckel (1972b) considered propulsion by photon reaction alone. This propulsion mechanism is much less efficient in producing thrust than is laser ablation, but it is capable of achieving relativistic speeds. It is interesting that Moeckel introduced the idea of using a 180-GW laser to propel a 10-tonne vehicle. However, he concluded that laser propulsion by photon reaction was not competitive, and with this we agree. Moeckel (1975) then picked up Kantrowitz's idea of using remotely generated laser power to heat propellant, in other words, propulsion by the much more efficient photoablation process, the concept of laser impulse space propulsion (LISP). He already realized that an optimum exhaust velocity exists for each flight mission that is proportional to the velocity change of the mission, and that the primary strength of LISP is that the optimum exhaust velocity can be selected and used. At that time, such proposals required large extrapolations of then existing technology, and the projected cost was prohibitive.

For a subject with such a long history, what has changed to account for the recent renaissance in interest? By the late 1970s, solid targets were being routinely accelerated to ever

 0263-0346/94 $5.00 + .00

increasing velocities ($v = c/1000$) as part of the laser fusion program. Kantrowitz' proposal gained credence. Driven largely by that program, the available energy per shot from pulsed lasers has grown by nine orders of magnitude in four decades: from millijoules in the 1960s to megajoules by the year 2000. As we shall see in Section 6, not all applications require unusually high energy: pulsed energies in the 100-J range with average power around 100 W could, even now, be useful for laser impulse station keeping (LISK). Propulsion from the ground, however, requires several MJ pulses per second kg (Phipps & Michaelis 1992).

While laser technology has grown to a level where only a relatively small increase in laser parameters is required for LISP and LISK, the need for this technology has increased dramatically. This need springs from the imminent clash between ecologists and the business community. This is not the place to enter into a discussion on the effect of chemical rockets on the ozone layer and their contribution to global warming; but there is little doubt that if the four major space programs attempt to continue at the present level, let alone expand, they will face considerable "green" political resistance. On the other hand, it must be remembered that the civilian satellite business represents several billion dollars in annual turnover. LISP and LISK might be the solution to this conflict of interests. In the next section we show that LISP could reduce the cost and pollution per launch, by an order of magnitude, whilst LISK could prolong the life of several multimillion dollar satellites (Ashoor *et al.* 1989). An added benefit of a LISP system would be its ability to induce reentry at a given time and place; this would enhance the chances of recovering valuable equipment and also reduce the ever-present risk of reentry in a populated zone.

The ultimate application of this work is shown in figure 1a. Because this application is very expensive to develop (in the neighborhood of \$10B), it will be the last of those we consider in this article to be realized, probably by the year 2020. This case is the one discussed in Section 5 and described in detail by the parameters in the middle column of table 3 of that section.

In figure 1, a 2.4-GW deuterium-fluoride (D-F) laser operating in a broad band centered at 4-μm wavelength is shown launching a 40-tonne object from earth to low-earth-orbit (LEO). The entire rear surface of the spacecraft is illuminated by the laser. The laser is repetitively pulsed (at 6 Hz in our example) to allow choice of the optimum intensity for the laser–surface interaction.

It may be "double-pulsed" as well (see figure 1c), that is, divided in time so that each laser pulse is composed of a pair of pulses, including a prepulse to set up the optimum density profile for absorbing the main pulse.

At launch, the object is shown suspended from a balloon platform at 35-km altitude to save the energy required to push through the majority of the earth's atmosphere. Although this is not a crucial feature of LISP, it has the further advantage of avoiding unnecessary opacity in the relationships among parameters in the analysis we will develop in this article. In fact, a Kennedy Spaceflight Center-type launch would not be the case with LISP: Some initial separation from the launch platform is necessary to protect launch optics from damage by the ablation jet.

The balloons are filled with hydrogen or methane, which is used as fuel by a small compressor that deflates the balloons and returns the assembly to earth after launch, saving most of the original lighter-than-air gas.

About 4 min are required to reach LEO. When it reaches LEO, the object will retain only 9.4 tonnes of its mass, nearly 31 tonnes having been boiled off by the laser beam in a rocket-like jet that drove the object into orbit. This "ablation jet" (primarily CO_2 and H_2O) would be much more benign than the reaction products of standard chemical rockets, for which the main requirement is high-energy density, with environmental friendliness a secondary, sometimes unattainable, goal.

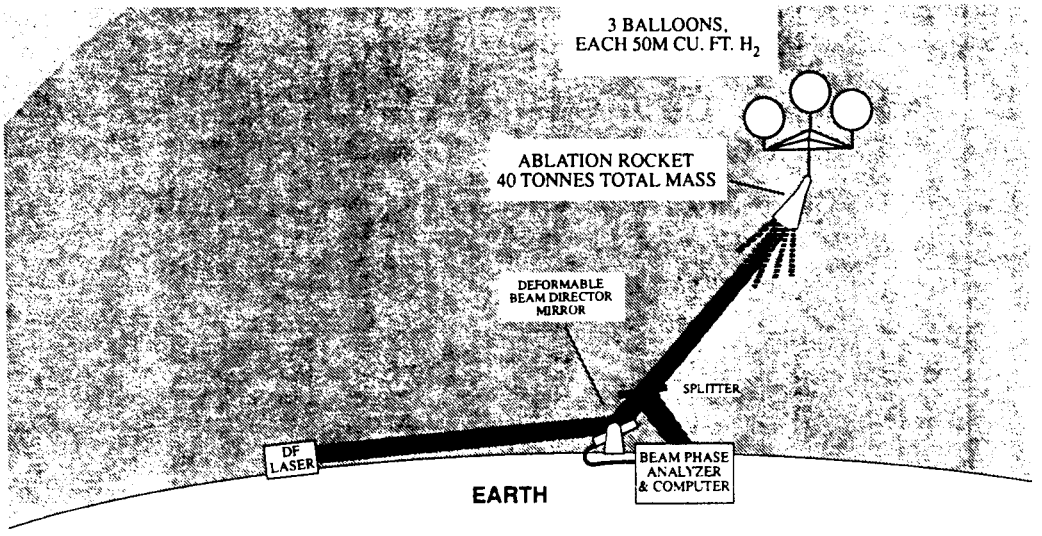

(A)

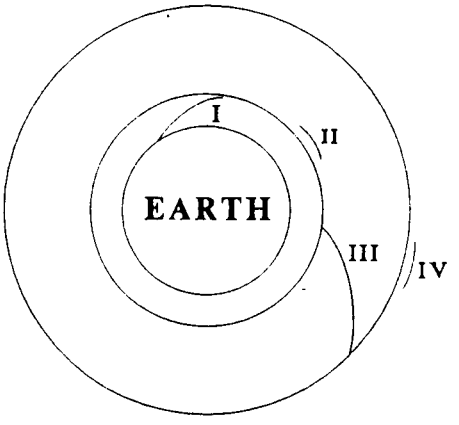

(B)

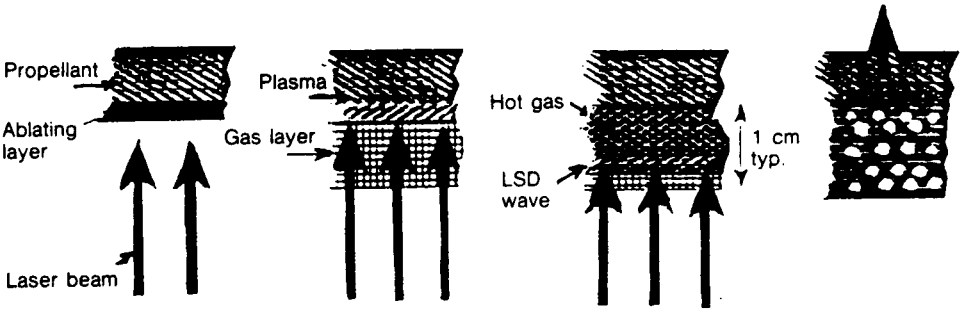

(C)

FIGURE 1. Various LISP geometries. (a) Balloon launch of ablation rocket from 35 km altitude (see Section 5). (b) The different LISP applications (see table 1). (I) Launch from ground (2020). (II) LO-LISP = LEO reboost (2010). (III) LEGO-LISP = LEO-to-GEO transfer (2000). (IV) LISK = geo-synchronous stationkeeping (1996). (c) Double pulse thrust cycle.

The DF laser is also environmentally friendly. It is a closed-cycle system in which the DF product is continuously electrolyzed into D_2 and F_2 with high efficiency. No products (not even the garbage of the electrolysis process) are vented to the atmosphere.

Table 1 and figure 1 summarize a variety of LISP applications. The difficulty of each task can be assessed from the estimated laser power required. The hardest task is launch from the ground. The easiest, geostationary orbit adjustment.

The answer to Kantrowitz' question, "Has its time come?" could be, "Not just yet; but this should be one of practical science's major goals for the decade."

2. Basic concepts and coupling theory

The science of LISP has grown from several preexisting disciplines. The basic concepts are a combination of laser fusion and rocket propulsion ideas developed in a number of laboratories. Laser propulsion suffers as much as any modern technology from a proliferation of abbreviations, symbols, and jargon. To help the transition from one field to another, we present in table 2 a list of abbreviations and symbols (with apologies for the occasional repetition or statement of the obvious).

Experiments with laser-induced acceleration of small bodies confirmed a pressure law

$$\mathcal{P} = 3.95 \frac{m_A^{0.44} I^{0.75}}{Z^{0.38}(Z+1)^{0.19}(\lambda\sqrt{\tau})^{0.25}} \quad \text{dyne/cm}^2, \tag{1}$$

where m_A is the mass number, Z the atomic number, λ the wavelength in cm, and τ the laser pulse width. The intensity I is in W/cm^2. Experiments indicated already in the early 1970s that velocities of orbital magnitude could easily be achieved.

The next step towards a practical method of acceleration came with the realization that using a laser to create a high-temperature plasma (tens of eV) is wasteful: too much energy goes into ionization and radiation. A better method would involve distributing the energy amongst a larger number of cooler particles. This led Reilly to suggest the double pulse cycle (Chapman *et al.* 1977).

A clear description of this process is to be found in Kare (1989). Essentially (see figure 1c) a first and somewhat weaker laser pulse evaporates a measured amount of propellant that creates a vapor shroud at a pressure of approximately 1 bar. A second, higher power pulse (possibly with an initial spike) penetrates unabsorbed through the vapor and ignites a thin high-energy plasma near the surface. As in laser fusion experiments, the solid surface of the foil is now quickly shielded from direct laser irradiation by the formation of a supercritical plasma density layer. At or near the outer edges of this layer, laser power is absorbed by inverse bremsstrahlung and a laser-supported detonation (LSD) shock wave forms (Raizer 1970). This heats the vapor uniformly to a moderate temperature of about 1 eV (ca. 10,000 K). When the LSD shock wave reaches the edge of the vapor, the laser pulse ceases and the hot gas expands, cools, and generates more thrust. The expansion is one-dimensional, giving rise to the description "planar thruster."

Some simple concepts and accompanying symbols and formulas occur frequently in LISP theory. The customary parameters used to describe laser momentum coupling to targets are in mixed units (but have an interesting "feel"):

- The momentum coupling efficiency C_m (the ratio of ablation momentum produced at the target surface to laser energy (dyne s/J)). Typically, C_m ranges from 1 to 100 dyne s/J.

TABLE 1. Near-earth LISP missions

LISP variant	Laser			Delivery optics
	Wavelength	Pulse format	Average power	
LISK: geosynchronous station keeping	530 nm	10 ns, 100 J, 1 Hz	100 W	3-m observatory telescope
LEGO-LISP: LEO-to-GEO transfer	800 nm	500 μs, 40 J, 250 Hz	10 kW	optical fibers
LO-LISP: LEO reboost	3–4 μm	50 μs, 20 kJ, 5 Hz	100 kW	3-m observatory telescope
LISK-BROOM: clearing space junk	0.5 μm	200 ns, 5 μs, 1 Hz	60 kW	5-m observatory telescope
LISP (ground): M = 40 tonnes, m = 1.6 tonnes	3–4 μm	50 μs, 215 MJ, 3 Hz	650 MW	7.5-m active optics

TABLE 2. LISP abbreviations and symbols

Abbreviations	
AERL	Avco Everett Research Laboratory
AIAA	American Institute of Aeronautics and Astronautics
DARPA	Defence Advanced Research Project Agency (now ARPA)
DF	Deuterium-fluoride
GEO	short for geostationary orbit
HF	Hydrogen fluoride
ICF	Inertial confinement fusion
KMS	Former Fusion Company
LANL	Los Alamos National Laboratory (New Mexico)
LEO	Low earth orbit
LEO-LISP	LISP launch from earth to LEO
LEGO-LISP	LEO to GEO LISP
LISK	Laser induced station keeping
LISK-BROOM	Space junk clearance
LLNL	Lawrence Livermore National Laboratory (California)
LO-LISP	LEO correction
LSD	Laser-supported detonation
MJ	Megajoule
NASA	National Aeronautics and Space Administration
NEO-LISP	Near-earth object LISP
NRL	Naval Research Laboratory (Washington, DC)
PMMA	Polymethylmethacrylate (lucite or perspex)
PSI	Physical Sciences Inc. (Andover, MA)
SDIO	Strategic Defence Initiative Office
SRS	Stimulated Raman scattering
TIA	Tuned ignition array
UCB	University of California (Berkeley)
UCLA	University of California (Los Angeles)

Physical Symbols, Constants, Units and Conversions

Quantity	Symbol	Practical cgs (this work)	SI
Average value of quantity	$\langle\ \rangle$	–	–
Laser beam area at satellite	A	cm^2, $\times 10^{-4}$ =	m^2
Intensity absorption coefficient	α	cm^{-1}, $\times 10^{2}$ =	m^{-1}
Frequency-dependent launch cost coefficient	B	\$ day/J	same
Thermal conductivity of a gas	χ	cm^2/s, $\times 10^{-4}$ =	m^2/s
Laser momentum coupling coefficient	C_m	dyne s/J, $\times 10^{-5}$ =	n s/J
Sound speed	c_s	cm/s, $\times 10^{-2}$ =	m/s
Normalization constant (Appendix)	$C_{x,y,z}$	s/cm, $\times 10^{2}$ =	s/m
Laser beam director diameter	D_1	cm, $\times 10^{-2}$ =	m
Satellite receiving aperture diameter	D_2	cm, $\times 10^{-2}$ =	m
Total impulse increment for mission	δJ	dyne s, $\times 10^{-5}$ =	n s
Areal mass density ablated per pulse	δm	g/cm^2, $\times 10$ =	kg/m^2
Momentum flux per puise	δp	dyne s/cm^2, $\times 10^{-1}$ =	n s/m^2
Laser beam diameter at target	d_s	cm, $\times 10^{-2}$ =	m
Velocity increment per pulse	δv	cm/s, $\times 10^{-2}$ =	m/s
Velocity increment for mission	Δv	cm/s, $\times 10^{-2}$ =	m/s
Kinetic energy flux of exhaust (Appendix)	e	erg/cm^2, $\times 10^{-3}$ =	J/cm^2
Laser fluence per pulse	Φ	J/cm^2, $\times 10^{4}$ =	J/m^2
Fixed launch cost coefficient	F	\$/J	\$/J
Laser repetition frequency	f	s^{-1}	s^{-1}
Velocity distribution (Appendix)	$f(v_x,v_y,v_z)$	–	–
Launch frequency	f_L	day^{-1}	day^{-1}

continued

TABLE 2. continued

Physical Symbols, Constants, Units and Conversions			
Quantity	Symbol	Practical cgs (this work)	SI
Thermal blooming gain	G	nepers	nepers
Acceleration of gravity	g	980.7 cm/s^2	9.807 m/s^2
Specific heat ratio c_p/c_v for a gas	γ	–	–
Laser ablation efficiency	η_{AB}	–	–
Laser intensity	I	W/cm^2, $\times 10^4$ =	W/m^2
Specific impulse	I_{sp}	s	s
Transverse spacial frequency	$k_\perp$	cm^{-1}, $\times 10^2$ =	m^{-1}
Boltzmann constant	k	1.38×10^{-16} erg/K, $\times 10^{-7}$ =	J/K
Laser wavelength	λ	cm, $\times 10^{-2}$ =	m
Drift Mach number, u/c_s	$\mathfrak{M}$	–	–
Mass at start of mission	M	g, $\times 10^{-3}$ =	kg
Mass at end of mission	m	g, $\times 10^{-3}$ =	kg
Atomic mass number	m_A	–	–
Exhaust particle mass	m_E	–	–
Laser pulse count during mission	N	–	–
Refractive index	n	–	–
Cosine exponent (Appendix)	v	–	–
Barnard distortion number	N_D	–	–
Price of laser light	P	$ per unit mass or energy	same
Pressure	$\mathcal{P}$	dyne/cm^2, $\times 0.1$ =	Pa
Average laser power	P_{ave}	W	W
Vector angle to surface normal	θ	degrees	degrees
Specific ablation energy	Q^*	J/g, $\times 10^3$ =	J/kg
Temperature (practical)	T	K	K
Laser pulse duration (FWHM)	τ	s	s
Flight time (powered)	t_F	s	s
Energy expended per unit mass	U	J/g, $\times 10^3$ =	J/kg
Drift velocity (Appendix)	u	cm/s, $\times 10^{-2}$ =	m/s
Velocity	v	cm/s, $\times 10^{-2}$ =	m/s
Laser energy	W	J	J
Ratio $\langle v_x^2\rangle/(\langle v_x\rangle)^2$ (Appendix)	Ψ	–	–
Average plasma ionization state	Z	–	–
Range	z	cm, $\times 10^{-2}$ =	m
Payload mass ratio M/m	ζ	–	–
Rayleigh range	z_R	cm, $\times 10^{-2}$ =	m
Siegman beam quality number	μ	–	–

- The specific ablation energy Q^* (the ratio of incident laser energy to mass removed from the target (J/g)). Typically, Q^* ranges from 10^3 to 10^5 J/g).

The parameters we will use throughout the following discussion are defined per unit area, except where explicitly noted otherwise. To agree with the majority of the existing literature in the fields of plasma and laser physics, as well as laser-surface interactions, units employed are practical cgs. Table 2 offers a conversion between these and SI units.

Ablation velocity v_E relative to the moving target (exhaust velocity) and ablated mass δm determine the impulse δp delivered to the target per pulse, which depends solely on laser and target parameters, not on their relative velocity:

$$\delta p = v_E \delta m \quad \text{dyne s/cm}^2. \tag{2}$$

Since

$$C_m \equiv \delta p/\Phi \quad \text{dyne s/J}, \tag{3}$$

where Φ is laser fluence,

$$Q^* \equiv \Phi/\delta m \quad \text{J/g}, \tag{4}$$

the quantity

$$C_m Q^* = \delta p/\delta m \equiv v_E \quad \text{cm/s} \tag{5}$$

is equal to the laser ablation exhaust velocity v_E taking the exhaust velocity distribution to be mono-energetic for analytical simplicity (see Appendix). Equation (5) is true *independent of laser energy coupling efficiency to the target*, because this efficiency cancels out in obtaining equation (5) from equations (3) and (4).

The so-called specific impulse for a simple, nozzle-less plane ablator is just

$$I_{sp} = v_E/\text{g} = C_m Q^*/\text{g} \quad \text{s}. \tag{6}$$

Meanwhile, the product $C_m I_{sp}$ is directly related to the efficiency with which laser energy is converted to ablation kinetic energy, since

$$\eta_{AB} = \frac{1}{2}\frac{\delta m v_E^2}{10^7 \cdot \Phi} = \frac{1}{2\cdot 10^7 \Phi}\frac{\Phi}{Q^*} C_m^2 Q^{*2} = \frac{C_m^2 Q^*}{2\cdot 10^7} = \frac{g C_m I_{sp}}{2\cdot 10^7}\ . \tag{7}$$

Equation (7) defines η_{AB}. It is obvious that this efficiency cannot exceed unity. The requirement $\eta_{AB} \leq 1$ gives:

$$C_m I_{sp} \leq 2\cdot 10^7/\text{g} = 20{,}394$$

and

$$C_m^2 Q^* \leq 2\cdot 10^7. \tag{8}$$

For launch of a payload to final velocity v_F in a gravity field g, the rocket equation is:

$$\zeta = M/m = \exp[(v_F + gt)/v_E]. \tag{9}$$

Since the thermal velocity of a 6000 K H_2O exhaust with average mass $A = 6$ is $2.88\cdot 10^7$ cm/s, equation (9) shows why the Space Shuttle tends to experience $\zeta \approx 16$. In laser ablation, plasma temperatures can be many times 10^4 K, and exhaust material can be chosen for optimum mission parameters rather than simply for combustion efficiency.

With $v_F = v_{\text{orbit}} = 7.72\cdot 10^5$ cm/s and employing equations (7) and (5), equation (9) gives, in practical terms

$$\zeta = M/m = \exp\left[\frac{v_F C_m}{2\cdot 10^7 \eta_{AB}}\left(1 + \frac{gt}{v_F}\right)\right] = \exp\left[\frac{C_m}{25.9\eta_{AB}}\left(1 + \frac{t}{787}\right)\right]. \tag{10a}$$

The factor 10^7 arises in conversion between joules and ergs. Equation (10a) can also be expressed in a form emphasizing the importance of I_{sp}:

$$\zeta = M/m = \exp\left[\frac{v_F}{g I_{sp}}\left(1 + \frac{gt}{v_F}\right)\right] = \exp\left[\frac{787}{I_{sp}}\left(1 + \frac{t}{787}\right)\right]. \tag{10b}$$

Equation (10) shows that the liftoff-to-orbit weight ratio M/m depends exponentially on the coupling coefficient C_m (or $1/I_{sp}$), and that $M/m \to 1$ as $\eta_{AB} \to 1$, flight time $t \ll 13$ min, and $C_m \ll 26$, or $I_{sp} \gg 787$.

Equation (10a) says that C_m cannot be too large, in other words, that we are not looking for exotic laser ablation materials in this program. Optimizing the cost of launch leads to similar choices for C_m with important differences in detail (see Section 4.2).

The time of flight t_F is given by the solution to the transcendental equation:

$$t_F = (MQ^*/f\Phi)[1 - 1/\zeta_F] \quad \text{s}, \tag{11}$$

where f is the laser pulse repetition rate (s^{-1}) and ζ_F is a function of t_F. With high exhaust velocity $v_E \gg v_F$, and short flights $t_F \ll 787$, equation (11) simplifies to

$$t_F \approx v_F M/C_m f\Phi \quad \text{s}, \tag{11a}$$

inversely proportional to the coupling coefficient, laser energy, and laser frequency. The energy expended per unit mass placed in orbit by N laser pulses is

$$U = N\Phi/m = Q^*(\zeta_F - 1) \quad \text{J/g}. \tag{12}$$

Levitation is achieved when

$$f = Mg/C_m\Phi \quad \text{Hz}. \tag{13}$$

I_{sp} *can be* the highest of all systems with laser ablation, as illustrated by comparing table 3 with figure 2. However, we will see that we do not want I_{sp} much larger than 600 s for the

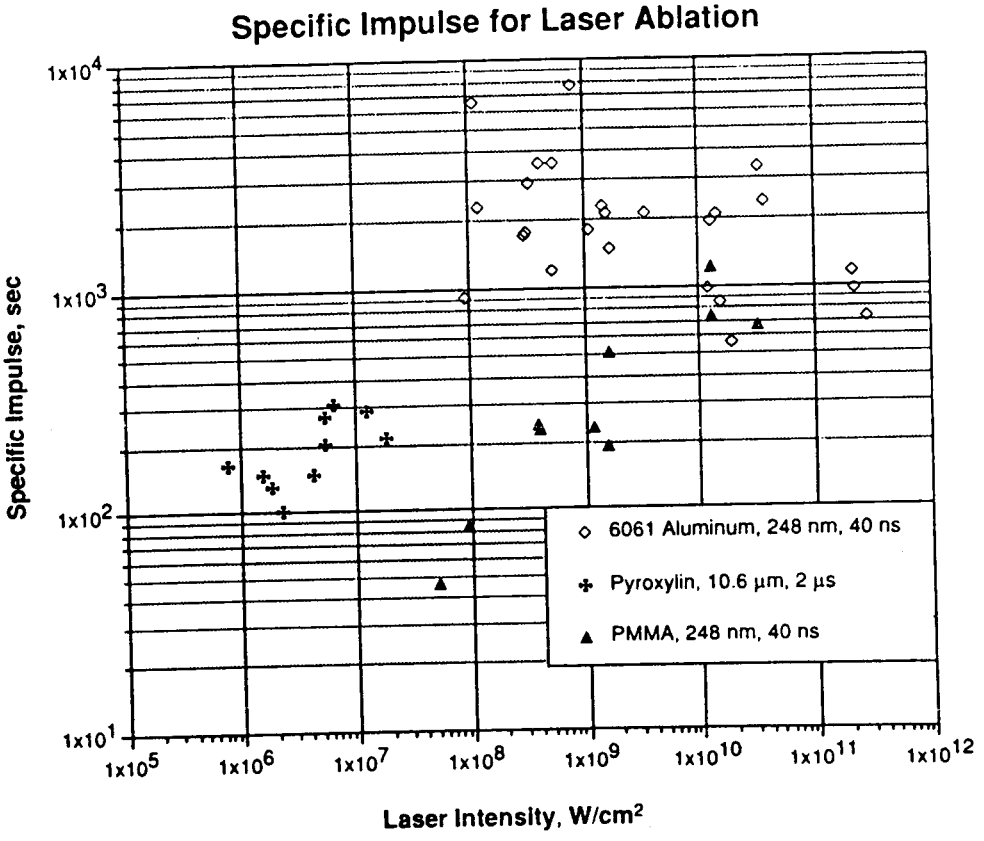

FIGURE 2. Survey of specific impulse measured with various intensities and materials.

TABLE 3. Specific impulse for various propulsion materials

Fuel or system	Specific impulse I_{sp} (s)
Aluminum at 1 GW/cm, 248 nm	2000-8000
PMMA at 10 GW/cm^2, 248 nm	700-1000
Nuclear thermal rocket	925
Hydrogen/fluorine	371
Oxygen/hydrogen	345
Pyroxylin at 10 MW/cm^2, 10.6 μm	300
Zinc/sulfur	20-50

earth-to-LEO mission. We have shown that I_{sp} should not be much larger than 300 s for LEO-to-GEO transport (Phipps & Michaelis 1992). Even lower I_{sp}, corresponding to very high C_m, is useful where very high acceleration is required or in small orbit changes at great distance, where a minimum cost of laser light delivered is the only economic concern.

Figure 2 demonstrates that laser ablation gives laboratory-measured specific impulse far exceeding values that can be obtained chemically, or have yet been obtained with nuclear thermal rockets, if such high I_{sp} is desired.

3. Laser impulse coupling advances

There are two distinct physical regimes in pulsed laser ablation. These are as follows.

3.1. *High* I_{sp} *with surface absorbers*[1]

For metals and other surface absorbers in vacuum well above the plasma formation threshold intensity, the same theory that produced equation (1) shows that I_{sp} can be determined fairly accurately given just the laser intensity I (W/cm^2), wavelength λ (cm), and pulse duration τ according to:

$$I_{sp} = C_m Q^*/g = 1400 f_{AZ} (I\lambda\sqrt{\tau})^{0.25} \quad \text{cm/s.} \tag{14}$$

The function $f_{AZ} \approx 1$ depends on the average plasma atomic mass number A and ionization state Z.

Figures 2-5 summarize our data for surface absorbers:

- We measured $I_{sp} \leq 8000$ s on 6061 alloy aluminium at 248 nm, and $I_{sp} = 1000$ s on PMMA at 248 nm.
- The C_m value consistent with these I_{sp} values in simple, surface-absorbing materials is low, about 3 dyne s/J.
- The ablation efficiency η_{AB} was low for most of the surface absorbers, except for aluminium, where the trend line approaches 50% at intensity near the plasma ignition threshold.
- At the same intensity, a factor of 5 enhancement in I_{sp} generated on aluminum is predicted from changing to 4-μm wavelength from 248 nm and 50-μs pulsewidth from 40 ns (figure 3). C_m will be about 1.3 at 4 μm.
- On glass with 10-μm wavelengths and 2-μs pulses, we found $I_{SP} = 400$ s at the same time that $C_m = 4.5$ dyne s/J, with $I = 15$ MW/cm^2.

[1]The second author (M. Michaelis) conducted early experiments (1974) with surface absorbers but had no part in generating the later results reported here.

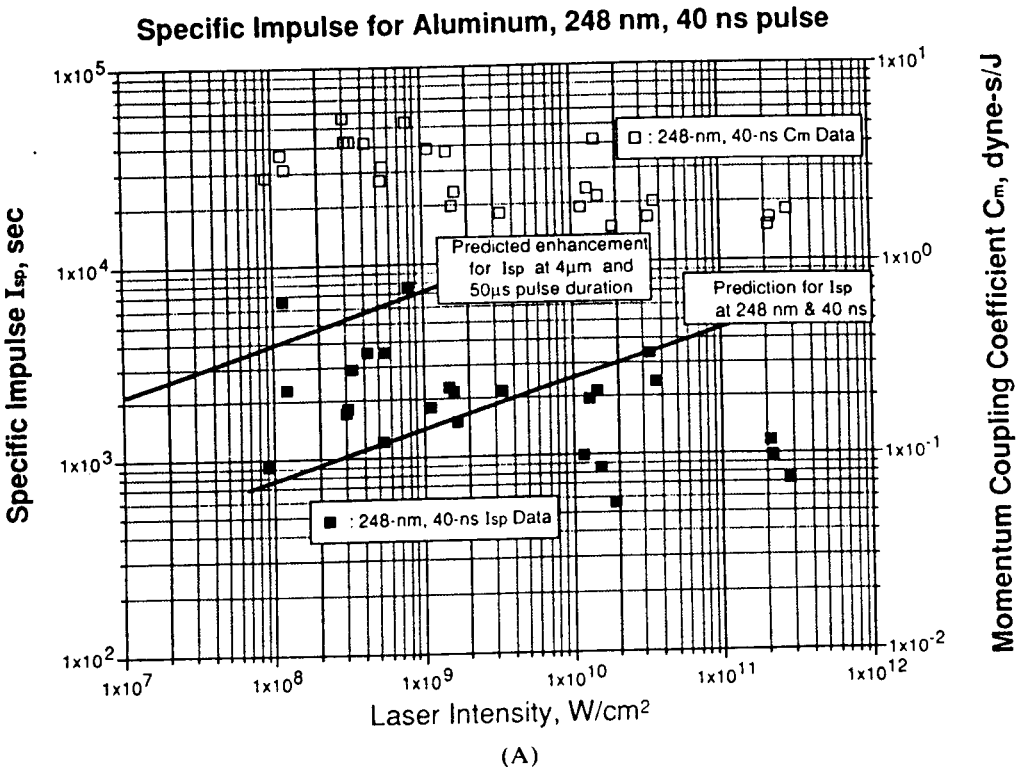

(A)

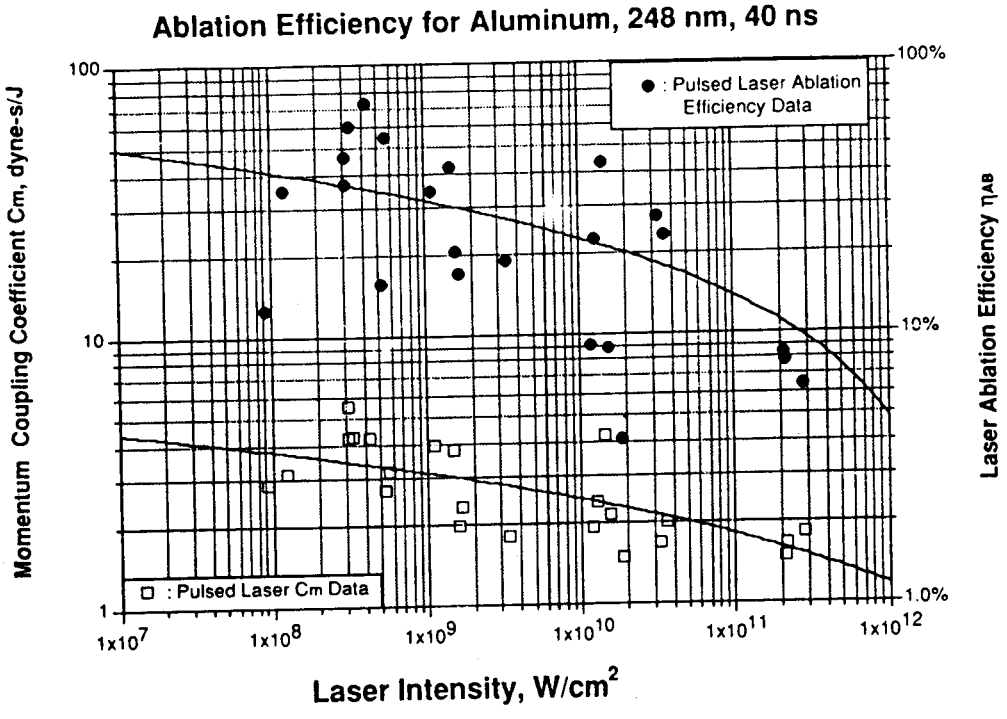

(B)

FIGURE 3. (a) Aluminium coupling data obtained with a pulsed KrF laser, compared to theoretical prediction for KrF and extrapolation to 50-μs pulse DF. (b) Data of part (a) reexpressed as ablation efficiency.

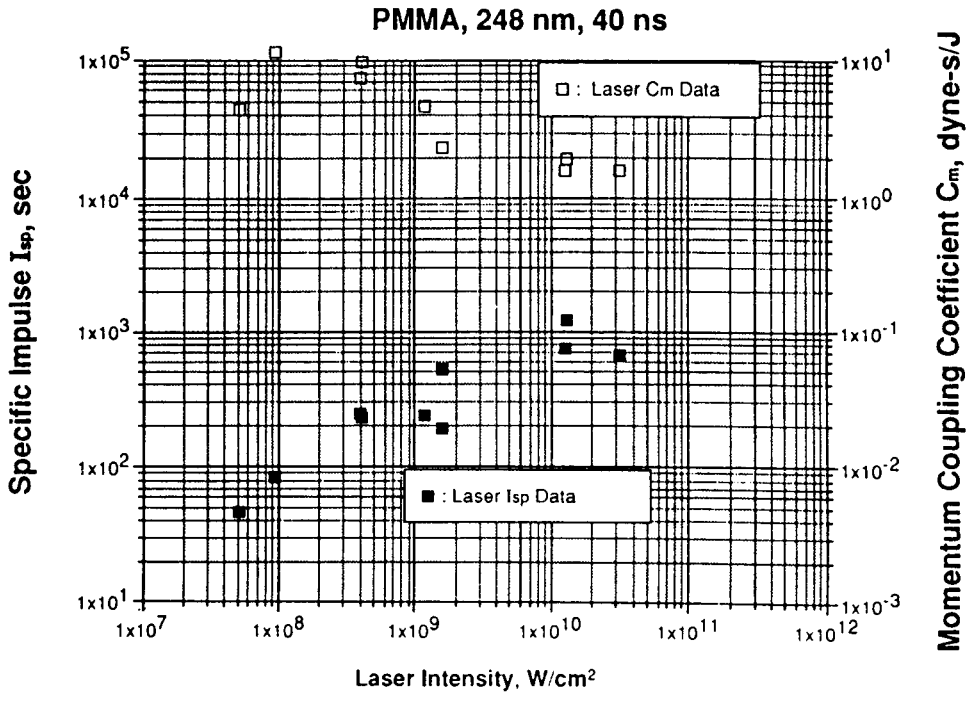

(A)

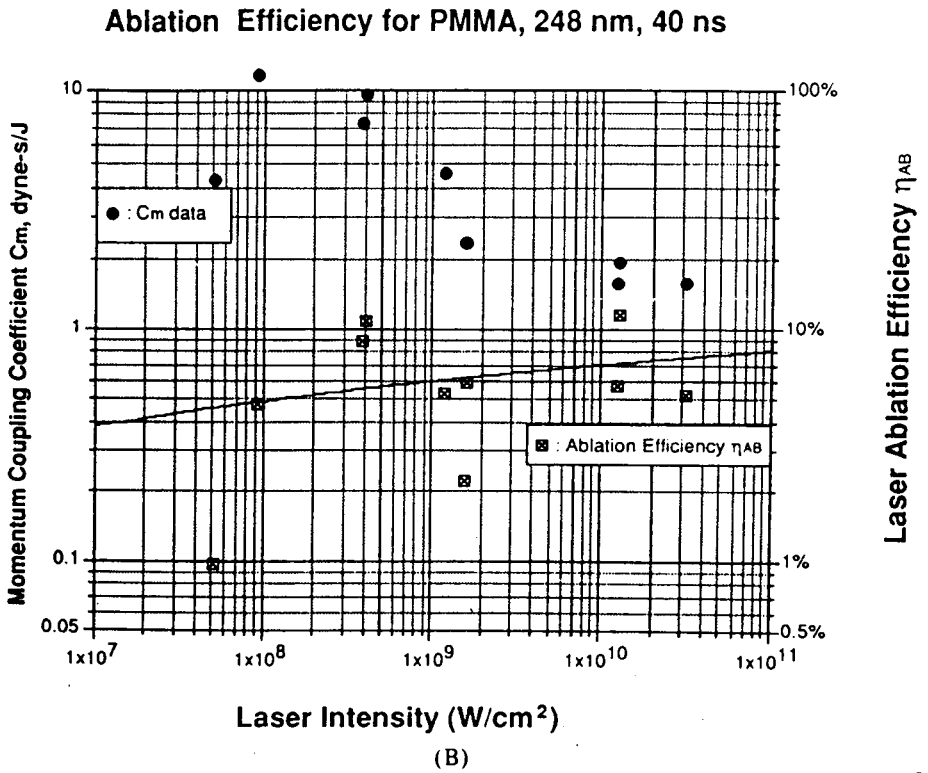

(B)

FIGURE 4. (a) KrF laser coupling data for PMMA. (b) Data of part (a) reexpressed as ablation efficiency.

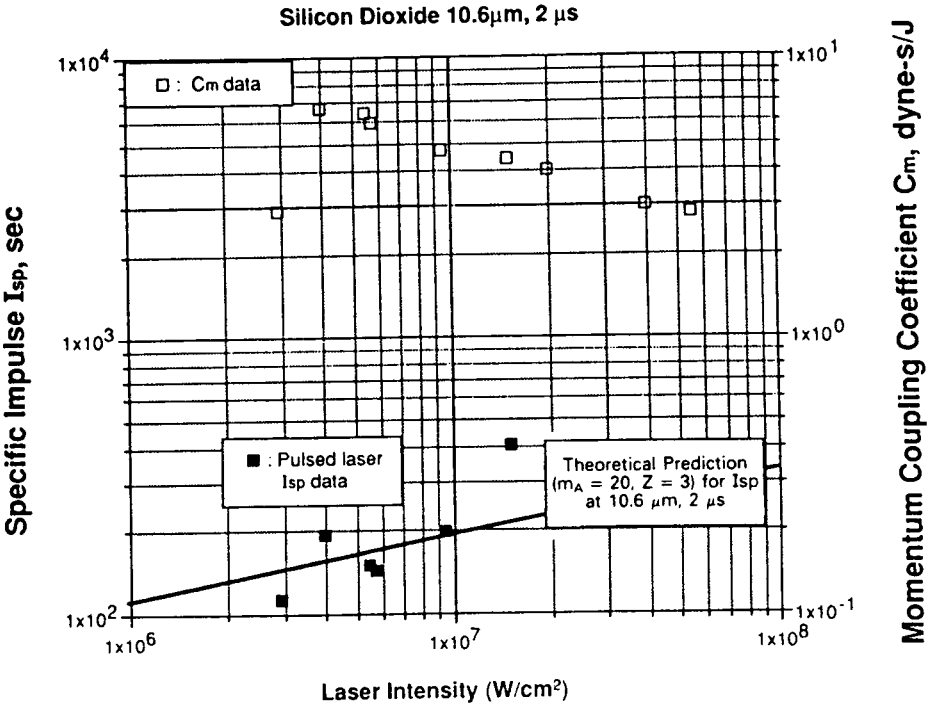

(A)

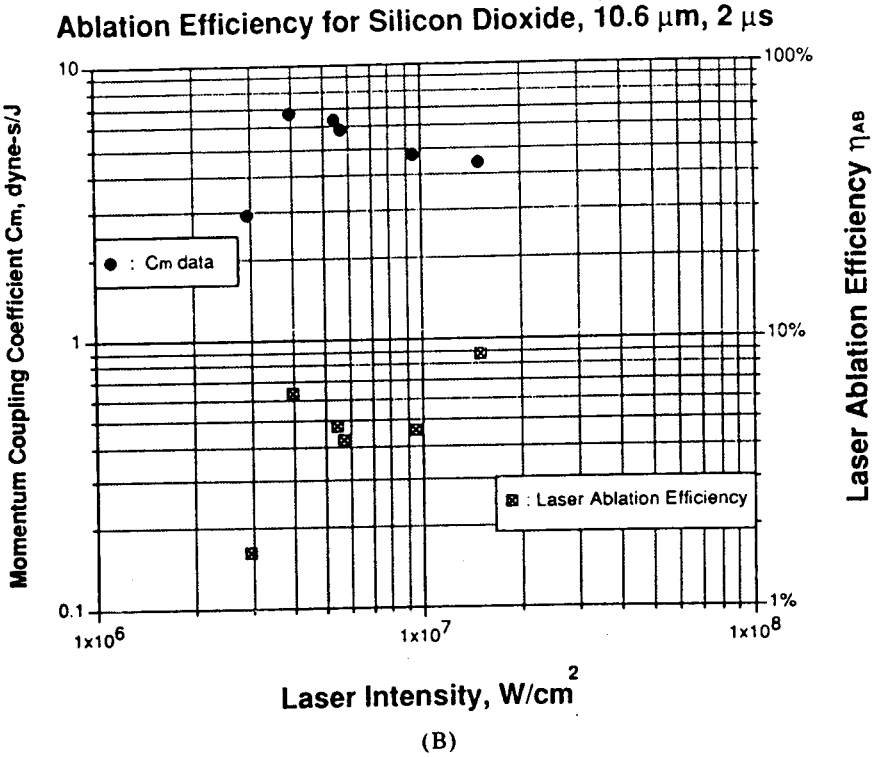

(B)

FIGURE 5. (a) CO_2 laser coupling data for glass. (b) Data of part (a) reexpressed as ablation efficiency.

We wish to limit laser beam intensity to 10 MW/cm^2 in the atmosphere, to minimize thermal blooming. In figures 3 and 4, we summarize our data for I_{sp} on aluminum and PMMA. It is seen that we have a trade-off within each data set: large C_m with low I_{sp}, or standard C_m with high I_{sp}. This behavior is predicted by surface-absorber coupling theory, as well as by equation (8), and is a consequence of energy conservation.

3.2. *High* C_m *with volume absorbers*

Volume absorbers are materials that benefit from trapped ablation (Phipps 1990; Fabbro *et al.* 1991), including both homogeneous, moderately absorptive materials, and complex stratified targets. A key feature of these data is the characteristic Q^* minimum in the intensity interval between efficient vaporization onset and development of plasma shielding (see figure 6). This Q^* minimum is located nearly opposite the C_m maximum, a feature that also results from plasma shielding.

In simple, homogeneous volume-absorbing materials, ablation trapping is a consequence of laser absorption throughout a finite absorption depth $1/\alpha$ (rather than just on the surface) that results in subsurface detonation.

Recently, there have been exciting advances in laser impulse coupling (Phipps *et al.* 1990) from work in this area: The largest coupling coefficients (90 dyne s/J) yet measured at that time for any laser wavelength or pulse width in vacuum were reported by Los Alamos work-

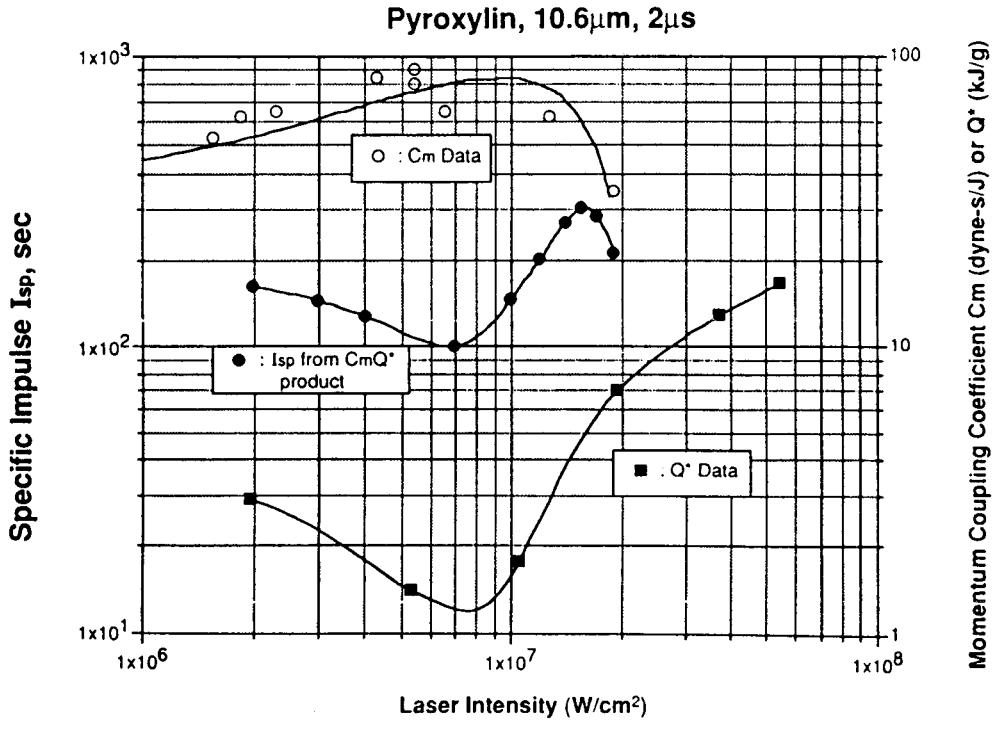

(A)

FIGURE 6. (a) Laser coupling data for the volume-absorber pyroxylin obtained with a 2-μs CO_2 laser. (b) Data of part (a) reexpressed as ablation efficiency. (c) Mjollnir pulsed HF laser vacuum data (3 μm, 1.8 μs). (*Figure continues*)

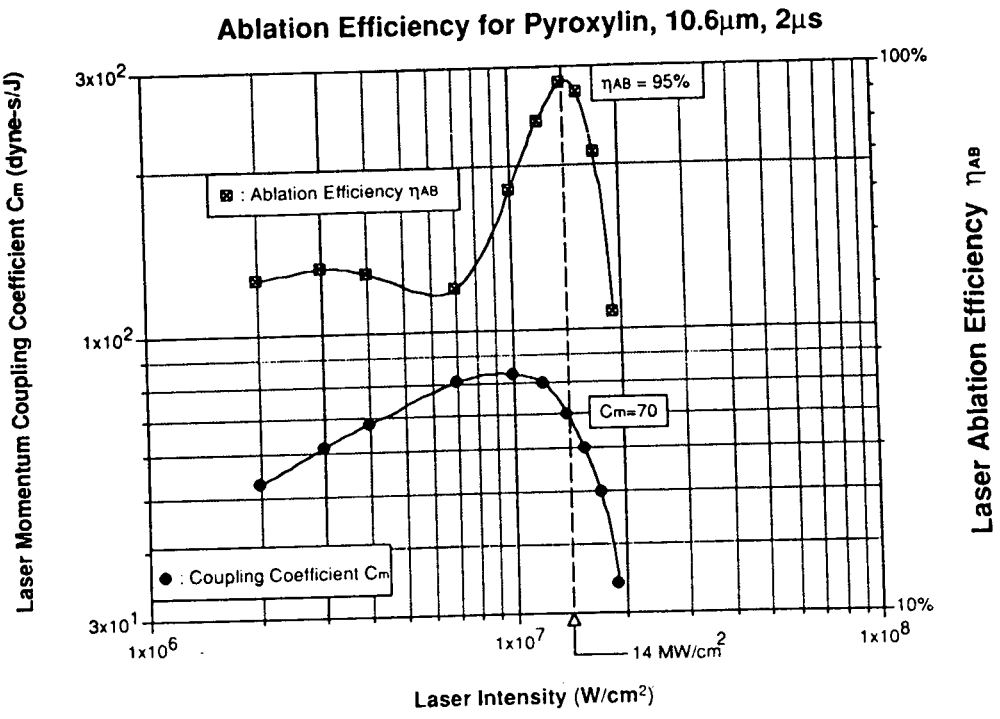

(B)

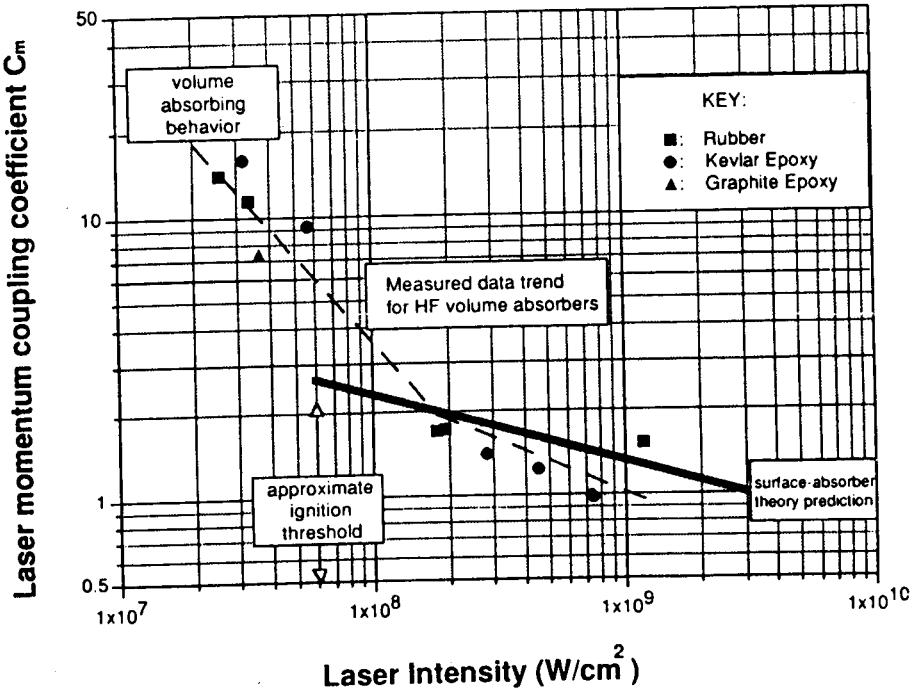

(C)

FIGURE 6 continued.

ers investigating volume-absorption vacuum ablation of pyroxylin by a pulsed CO_2 laser (figures 6a and 6b). Large C_m values are important, since the laser energy required to lift a vehicle is inversely proportional to C_m.

However, the most important feature of the data presented in figure 6a is that it shows attainment of 95% efficiency in the conversion of laser energy to ablation kinetic energy. This is probably the first time such behavior has been clearly seen, and it is a crucial basis element for our LISP concepts.

Volume-absorbing behavior was first identified in our work with HF lasers. We observed (figure 6c) that C_m values obtained with several nonmetallic targets were nearly an order of magnitude larger than predicted by the surface-absorber theory. It is important to note that C_m values as large as 17 dyne s/J have been obtained at 3-μm wavelengths from simple, homogeneous materials.

We have done a lot of the work in this interesting area over the past decade, and our work in laser impulse coupling theory (Phipps 1989; Phipps *et al.* 1990) and measurements (Phipps *et al.* 1988) has become well known. Nevertheless, it is clear that much remains to be done to better understand and measure infrared laser momentum coupling and mass removal rates.

4. The high-efficiency DF laser

Infrared lasers are the best choice for heavy-lift space propulsion for four reasons:

1. optimum atmospheric transparency;
2. unequalled electrical efficiency;
3. by far, the lowest cost per unit output;
4. unexcelled momentum coupling efficiency to targets and intensities appropriate for transmission through the atmosphere.

Since equation (1) shows that for plasma threshold surface absorbers, $C_m = P/I \approx (I\lambda\sqrt{\tau})^{-0.25}$, it is clear that for the same intensity and pulse width, shorter wavelength gives better coupling. However, volume absorbers in the infrared have given the largest coupling coefficients yet seen in vacuum.

Analysis shows (Phipps 1990c) that the cost of pulsed laser electrical power subsystems is the main factor in high-energy laser cost, followed by the cost of optics. Laser electrical efficiency is therefore a major consideration. Chemical laser demonstrations at Los Alamos have demonstrated electrical efficiency in excess of 1000% in the 10-μm DF-CO_2 transfer electron-beam-initiated laser (York 1991), 100–1000 times larger than for the best conventional lasers, and a laser technology breakthrough. Electrical efficiency η_E is the ratio of laser energy output to the electrical energy required to initiate the chemical reaction uniformly and quickly to produce the desired laser pulse duration. Since most of the laser pulse energy is derived from chemical energy, we can have $\eta_E > 1.0$. This is not a frivolous statement, since the cost of pulsed electrical energy (including electron-beam guns and pulsed electrical power supplies) dominates the cost of chemical energy and is a main determinant of laser cost, the other being the cost of optics. The main reason this laser can be so inexpensive compared to other types is that most of its output is not derived from pulsed electron beams. The 4-μm DF laser maintains the electrical efficiency of the DF-CO_2 transfer laser (by eliminating the vibrational transfer step) while being better able to focus at large distances.

This efficiency derives, in part, from using very long (50 μs) laser pulses in high-gain laser cavity configurations to extract all the available inversion energy. As a serendipitous ben-

efit, this pulse width is nearly optimum for efficient momentum generation on solid targets (Phipps *et al.* 1988).

With the advent of the efficient long-pulse HF/DF laser have come concepts for the minimization of large optics (Phipps 1989), reducing the other significant component of high-energy laser cost.

4.1. *Which wavelength is best?*

For the ground-based LISP concept, minimizing atmospheric attenuation and the attendant thermal blooming instability are crucial considerations. The total atmospheric attenuation of various laser wavelengths, averaged over the indicated number of lines, is indicated in table 4. Shorter wavelengths than those shown are attenuated even more strongly by sea-level aerosols. It is seen that DF is the best wavelength for propagation to space. Our design philosophy is not merely addressed to avoiding energy loss. Absorption heats the air, inducing "thermal blooming" of the beam due to thermal refraction, and convective-turbulent distortions over a number of pulses. Even with DF, 1.2 kW/m^3 will be absorbed from the beam by sea-level air, but, over most of the path, the absorbed power density is $\leq$70 W/m^3.

We do not believe there is a problem from conversion by stimulated Raman scattering (SRS) in the atmosphere at 10 MW/cm^2 and 4-μm wavelength. Further study of multiline spectrum effects is planned in our proposed research program to see how effectively the separate wavelengths cooperate in producing SRS, relaxing the intensity limit posed by SRS. However, we have chosen our beam intensity assuming complete cooperation. We note that the SRS beam-intensity limitation is proportionally more stringent at shorter wavelengths, giving a definite advantage to DF.

The final consideration affecting wavelength choice has to do with focusing optic size as it relates to propagation range z. In the Kogelnik–Li theory (Kogelnik & Li 1966) governing Gaussian beam propagation, the expression governing these quantities is

$$D = 2\sqrt{2}\sqrt{\mu\lambda z/\pi} = \sqrt{2}d_s \quad \text{cm}, \tag{15}$$

where the beam is μ times diffraction limited, d_s is the spot size at the beam waist on the distant object, z is the range, and D is the mirror diameter. The sacrifice for using a 4-μm wavelength is not severe for LEO–LISP applications.

4.2. *DF laser cost*

The cost of the high-efficiency DF pulsed laser is considerably smaller than the cost of conventional lasers of the same pulse energy. Our studies have indicated that MJ-class lasers using standard optics can be built for about \$10/J of pulsed output. Our studies suggest that a 100-MJ single-pulse laser will be substantially cheaper than \$10/J. This figure for high-efficiency long-pulse chemical lasers is surprising but credible for three reasons:

TABLE 4. Which wavelength is best?

Laser	Wavelength (μm)	α, Sea level (km^{-1})	α at 12 km (km^{-1})	No. lines
CO_2	10	0.0715	0.0078	41
HF	3	0.122	0.00036	10
DF	4	0.0403	0.0023	63
Nd:GLASS	1.06	0.05	0.01	1

1. The few optics that do exist (an unstable resonator mirror set and an output window) can be 30 times smaller per output joule relative to the short-pulse case, because of the increase of optical damage threshold of metal mirrors with increasing pulse duration.
2. We are more accustomed to costs around \$1000/J for large-pulsed laser systems, but these apply to very-short-pulse (typically 10 ns) lasers for fusion. The amount of pulsed electrical initiation energy required ranges from about 7 kJ/L (Phipps 1990c) for short-pulse Nd:glass lasers to 100 J/L (Phipps 1989) for chemical ICF lasers. For the DF chemical laser we propose for LISP, the initiation energy is 100 times smaller at about 1 J/L. Pulsed power being the dominant cost factor in a laser with few optical components, the 100-times-smaller laser cost derives to first order from a 100-times-smaller pulsed power requirement. Stated another way, the cost per stored *electrical* joule is about the same as in other laser concepts.
3. It is well known that the unit cost decreases with larger devices. Cost studies for the Meteor series of DF lasers (Phipps 1990d) suggest that a 100-MJ single-pulse laser will be substantially cheaper than \$10/J, which was estimated for a 1-MJ laser. We think that the higher unit cost of the repetitively pulsed capability required for LISP will be counterbalanced by the unit cost reduction due to scaling from 1 to 100 MJ per pulse.

Chemical energy cost is, of course, the most significant component of the launch cost. The energy cost for one 100-MJ laser shot is about \$200. This figure is achieved by efficient electrolysis of the DF reaction product, plus postprocessing the electrolysis byproducts to nearly eliminate consumption of D_2. Including the fact that the DF laser's chemical efficiency (light output divided by chemical energy input) is 7%, the operational energy cost is \$0.14 per MJ of primary energy, or \$2 per MJ of light energy, compared to about \$0.02 per MJ current cost of commercial electrical energy. It is apparent that the cost per pound depends upon launch frequency as well as I_{sp} and C_m.

For reasons given above, we analyze launch price per joule in this range of energy as being composed of a fixed component, plus a component that decreases with launch frequency $f_L(\text{day}^{-1})$:

$$P = F + B/f_L \quad \$/\text{J} \tag{16a}$$

and is calculated following, where f_L is the daily launch rate.

For the 150 GJ invovled in a typical launch using 1500 pulses from a laser capable of 100 MJ per pulse, we estimate:

- Laser consumables \$300k
- Ablator \$70k
- Facility amortization \$500k/f
- Crew \$150k/f

from which we take $F = 2.47 \cdot 10^{-6}$ and $B = 4.33 \cdot 10^{-6}$, using linear scaling, a conservative assumption as laser size increases. Facility amortization costs are based on a total facility cost of \$3B at 5% of the annual interest rate.

Now the cost per unit mass lifted into orbit is given by

$$PU = Q^*(F + B/f_L)(\zeta_F - 1) \quad \$/\text{g}. \tag{16b}$$

Substituting equations (10b) and (11) into equation (16), we find:

$$PU = \frac{1 \cdot 10^4 \eta_{AB}}{C_m^2}\left(2.240 + \frac{3.92}{f_L}\right)\left\{\exp\left[\frac{v_F C_m}{2 \cdot 10^7 \eta_{AB}}\left(1 + \frac{g t_F}{v_F}\right)\right] - 1\right\} \quad \$/\text{lb}, \tag{17}$$

TABLE 5. Minimum LEO cost ($/lb) with optimum ablation parameters

Launch frequency	Cost
1	142
2	97
7	64
100	52

where v_F and t_F are parameters at LEO insertion. To find the ideal coupling coefficient in terms of cost per pound into LEO, we differentiate equation (17) and find that there is a definite minimum, given by the solution of the transcendental equation:

$$bC_m = -\ln(1 - bC_m/2) \tag{18}$$

the solution of which is $C_m = 1.59/b$, where

$$b = \frac{v_F}{2 \cdot 10^7 \eta_{AB}} \left(1 + \frac{t_F}{787}\right). \tag{18a}$$

In other words, *the ideal coupling coefficient* $C_m = 41.3$ dyne s/J for short flights to LEO ($t_F \ll 13$ min), about 33 dyne s/J for realistic t_F, and either higher or lower C_m values are quite costly. Energy conservation [equation (8)] then requires that $I_{sp} \approx 500$. Results for the minimum launch cost to LED are given vs. launch frequency in table 5.

Equation (17), behaving like $\exp(C_m)/C_m^2$, changes rapidly around the minimum (see figure 7) and is already 90% above minimum cost when $C_m = 100$ and again when $C_m =$

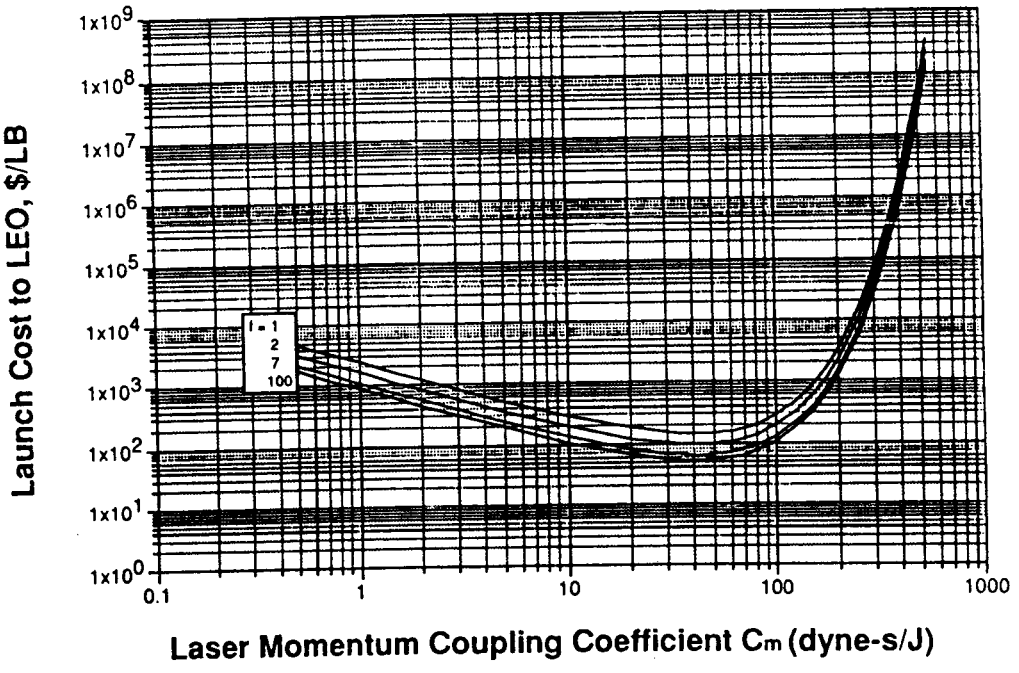

FIGURE 7. Unit LEO launch cost as influenced by laser coupling coefficient C_m.

10. For $C_m = 1$, the cost factor is about 17 times the minimum cost. These data are combined in the calculations leading to figure 7, which shows cost per pound from earth into LEO using DF-laser LISP reaching \$77/lb at $f_L = 7$ launches per day. Not much improvement (\$63/lb) is obtained by going to 100 launches per day.

Figure 7 shows that the demonstrated performance of pyroxylin volume absorbers [$C_m = 65$ dyne s/J at $\eta_{AB} = 95\%$] is already more than adequate (at 10-μm wavelength) to drive the cost of LEO launch to \$50/lb. The best mass ratio, $\zeta = M/m$, which is deliverable with C_m chosen for optimum cost [equation (10a)], is exp(1.59) = 4.88.

4.3. *Beam directors and thermal blooming*

Figure 8 illustrates the method of operation of an active phase conjugation system developed by Minneapolis-Honeywell for Lockheed (Mehta 1992). This is the first system that has sufficient bandwidth (about 1 kHz) to match the bandwidth of atmospheric scintillations.

We have addressed the thermal blooming instability by applying the recent detailed theory of Barnard (1989). For laser pulses in the μs regime, there are four regimes of interest as the transverse spatial frequency of the initial beam intensity perturbation increases from those of whole-beam effects to ripples on the order of 1 mm. Exponential gain G for perturbations of spatial frequency $k_\perp$ is given by four expressions that fold smoothly into each other at boundaries between regions of applicability.

In equation (19), (see table 6) χ is the thermal conductivity of the atmosphere, about 0.22 cm^2/s, z is the range (cm), τ is the actual laser pulse duration (s), $k = 2\pi/\lambda$, λ is the laser wavelength (cm), and I_0 is the laser beam intensity (W/cm^2). The parameters are refractive index $(n - 1) = 2.68 \cdot 10^{-4}$, specific heat ratio $\gamma = 1.393$ (Eshbach 1952), $k = 2\pi/\lambda$, and the intensity absorption coefficient α (cm^{-1}) is given in table 4.

The important point about this progression is that the gain for high-spatial-frequency transverse beam perturbations first increases proportionally to $k_\perp^{1/2}$ but ultimately satu-

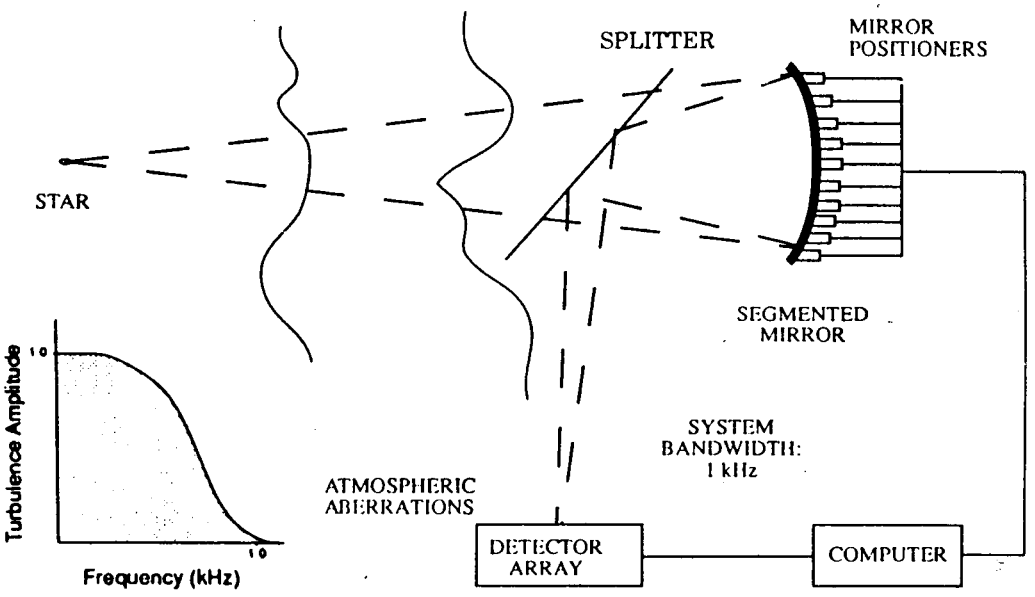

FIGURE 8. Illustrating active phase correction of an optical path with 1-kHz bandwidth.

TABLE 6. Gain for thermal blooming and inhomogeneties

	$k_\perp$ condition	Exponential gain G	
a. and	$k_\perp \ll 1.96[(n-1)I_0\alpha c_s^4 k^5]^{1.6}(\tau/z)^{1/2}$ and $k_\perp \ll 1.27[(n-1)I_0\alpha z^2/c_s^3\tau^2]$	$G = 1.88[(n-1)\alpha c_s^2 z^2 I_0 \tau^3 k_\perp^4]^{1/5}$	(19a)
b. but	$k_\perp \gg 1.96[(n-1)I_0\alpha c_s^4 k^5]^{1.6}(\tau/z)^{1/2}$ but $k_\perp \ll 1.59[(n-1)I_0\alpha kz/c_s^2\tau]^{1/2}$	$G = 2.02[(n-1)\alpha c_s^2 kz I_0 \tau^3 k_\perp^2]^{1/4}$	(19b)
c. and	$k_\perp \gg 1.78[(n-1)I_0\alpha\tau k^3/z]^{1/4}$ and $k_\perp \gg 1.59[(n-1)I_0\alpha kz/c_s^2\tau]^{1/2}$	$G = 2.22[(n-1)\alpha I_0 kz\tau]^{1/2}$	(19c)
d.	$k_\perp \gg [G/\tau\chi]^{1/2}$	Grating washout by thermal diffusion	(19d)

rates, becoming independent of $k_\perp$ as $k_\perp$ increases. As can be seen from figure 9, gain G does reach 10 for millimetric ripples of 6 MW/cm^2 intensity levels, just before reaching the smallest scale, where the index grating washes out by thermal diffusion. In figure 10 and table 6, Barnard's terminology is defined as follows:

$$N_D = 2.53(n-1)\alpha I_0 kz\tau, \quad \text{the "distortion" number,} \tag{20}$$

$$\tau = \sqrt{2k/z}\, c_s\tau, \quad \text{a reduced pulse duration.} \tag{21}$$

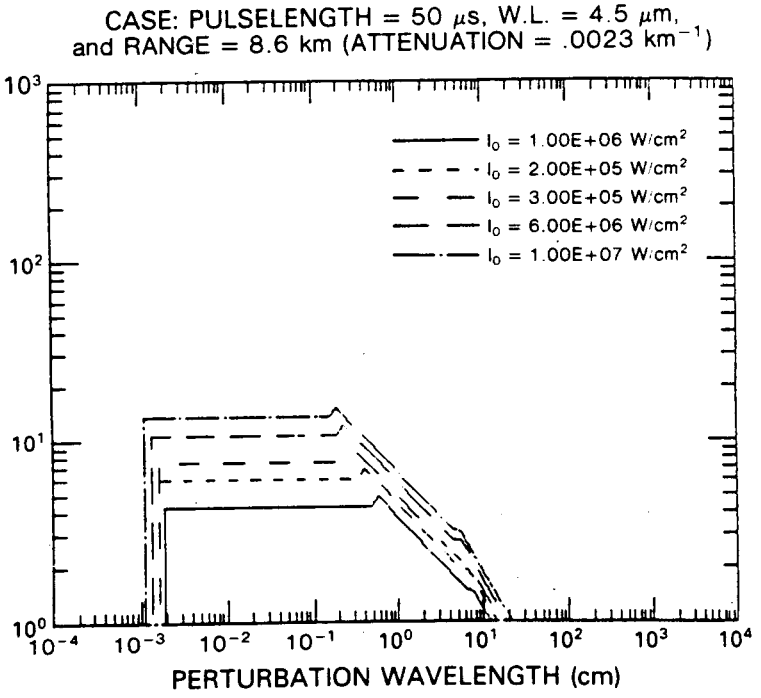

FIGURE 9. Exponential gain for intensity perturbations, calculated from the Barnard theory versus wavelength for a range of intensities.

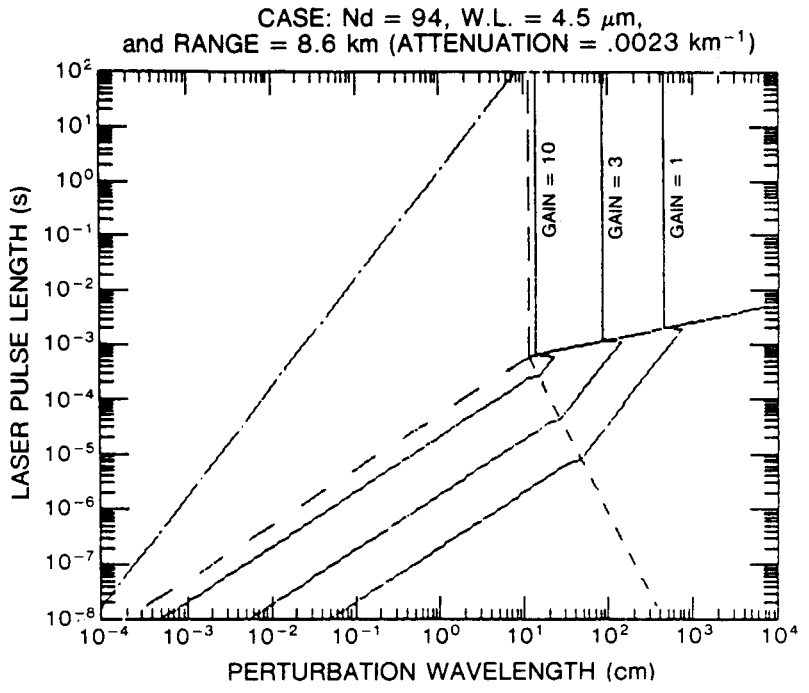

FIGURE 10. Calculation for fixed 10-MW/cm^2 intensity: follow the solid lines for thermal blooming gains 1, 3, or 10 to determine how pulse length affects the problem.

We can propagate the laser beam with a beam director having a reasonable diameter. The active mirror segments implicitly correct mirror shape errors inherent in large mirrors. A 1-kHz active mirror system was demonstrated at the solar observatory at Sacramento Peak, New Mexico, to correct the optical path in ground-based astronomy to a level of 1/3 arc second, which approaches the optical quality that would have been achieved by the Hubble telescope above the atmosphere and is equal to the vacuum diffraction-limited performance of a 6-m-diameter mirror at 4-μm wavelength (Acton & Smithson 1989).

5. Ground-based LISP example

We did a typical design, for which the parameters are listed in the first column of table 7 and shown in figures 11 and 12. To start a 40-tonne object on its orbital trajectory in a one-gravity field, it is necessary to develop $\delta J = 6.5 \cdot 10^9$ dyne s at a rate $f = 6$ Hz (see figure 1a for flight configuration).

To illustrate the importance of the value of C_m, equations (2) and (12) show that, if we pick a typical surface absorber with $C_m = 1.3$, the laser energy W must be 5 GJ. If instead we have $C_m = 70$, keeping f constant at 6 Hz, then W need only be 90 MJ. At \$10/J, the latter laser would cost less than \$1B to build.

We also did a number of orbit calculations using a simple code we developed for the purpose, which are summarized in Table 7. In the first column of the table we assume interaction parameters that have already been demonstrated. We used pyroxylin parameters $C_m = 70$ dyne s/J, $I_{sp} = 286$ s ($Q^* = 4$ kJ/g), a 215-MJ, 50-μs pulse, a 3-Hz DF laser that provides a 7.5-m-diameter beam in the lower atmosphere, and 750 J/cm^2 fluence at the

TABLE 7. Three test cases for laser launch into LEO

Case	I		II		III	
Laser						
Pulsewidth (μs)	50		50		50	
Wavelength (μm)	4–5		4–5		4–5	
Energy (MJ)	214		400		13,100	
Repetition rate (Hz)	3		6		6	
Lines in spectrum	30		30		30	
Beam, based on WINDOW TYPE	AERO	(SOLID)	AERO	(SOLID)	AERO	(SOLID)
Diameter D_a in atmosphere (m)	7.4	(20)	10.1	(27)	58	(1300)
Pulse fluence in atmosphere (J/cm^2)	500	(66)	500	(66)	500	(66)
Peak intensity in atmosphere (MW/cm^2)	10	(1.32)	10	(1.32)	10	(1.32)
Diameter D_t at target (cm)	600		820		1,830	
Pulse fluence at target (kJ/cm^2)	0.75		0.75		5	
Peak intensity at target (MW/cm^2)	15		15		100	
Average intensity at target (kW/cm^2)	2.3		2.3		30	
Transient thermal blooming						
Mean attenuation (km^{-1})	0.0023		0.0023		0.0023	
Effective path length (km)	8.6		8.6		8.6	
Mean intensity (MW/cm^2)	10	(1.32)	7.94	(1.32)	10	(1.32)
N_D (Barnard's distortion number)	94	(12.4)	94	(12.4)	94	(12.4)
τ (Barnard's reduced pulse duration)	0.27		0.27		0.27	
Gain [whole beam SF, $\lambda_\perp = (D_a/2)$] (nepers)	0.09	(0.06)	0.09	(0.06)	0.02	(0.001)
Gain [10 μm $\leq \lambda_\perp \leq$ 2 mm] (nepers)	14	(5)	14	(5)	14	(5)
Launch parameters						
Ablator material	pyroxylin		R&D target		6061 Aluminum	Shuttle
C_m (dyne s/J)	70		33		1.3	
Q^* (J/g)	4000		18,400		2.3×10^6	
I_{sp} (s)	286		620		3,060	295
Initial mass (tonnes)	40		40		40	2000
Initial altitude (km)	30		35		30	
Mass to LEO (tonnes)	1.64		9.44		29.7	125
Payload mass ratio	24.4		4.24		1.35	16
Time to LEO (s)	240		233		303	
Energy to LEO (GJ)	154		561		23,790	
Orbit [max X min altitude] (km)	377 × 126		189 × 164		185 × 169	

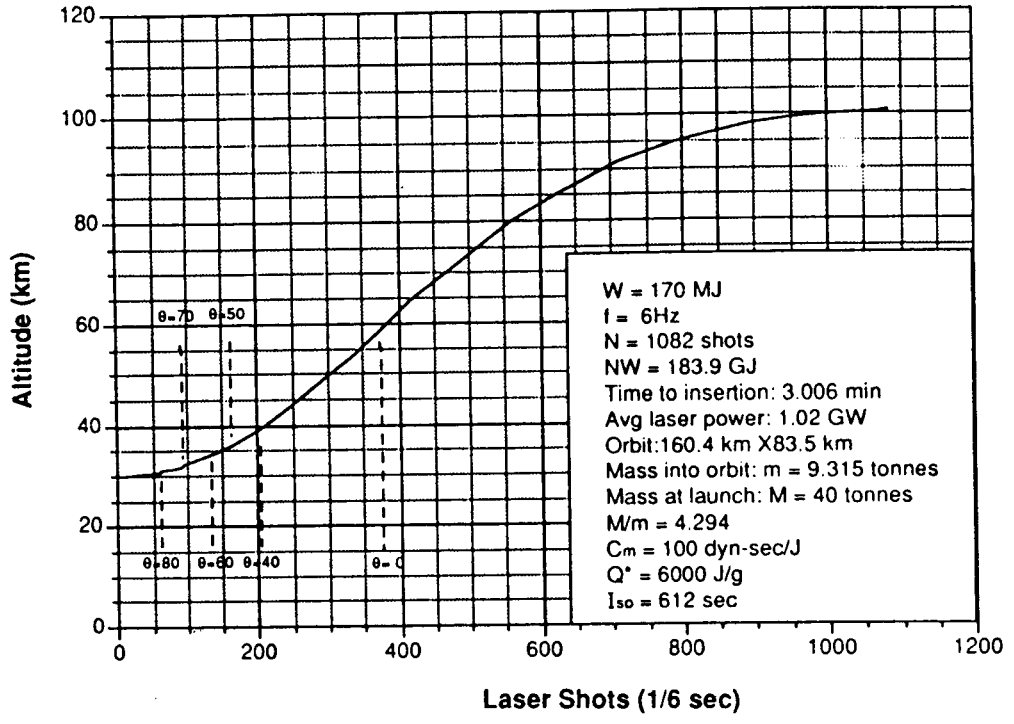

FIGURE 11. Calculated launch profile versus time.

target (intensity 15 MW/cm^2). With a 4-tonne vehicle initially suspended at 35 km altitude, we obtained orbital insertion into LEO of $m = 1.6$ tonnes in 4 min using 716 shots from the laser (153 GJ). In this simulated launch, $\zeta = M/m$ was 25.

In the case outlined in the second column of table 7, we picked $C_m = 33$, which is the optimum given by equation (18a) when nonzero time of flight is taken into account. The corresponding $I_{sp} = 620$ s. This reduction in the coupling coefficient led to a factor of 5.8 improvement in mass delivered to LEO, with $m = 9.4$ tonnes and $\zeta = 4.2$. The energy cost of delivering a pound of mass to LEO was 60% higher in column 1 than in column 2.

In the third case, we used aluminum to illustrate both the strong advantages and disadvantages of metallic or "surface" absorbers. For the improvement in I_{sp} we paid a large sacrifice of almost a factor of 100 in C_m. The result is an impressive payload mass ratio of 1.35 (30 tonnes into LEO), but also the requirement for 24 TJ for orbital insertion, corresponding to a monstrous, 13-GJ-per-pulse laser with a 60-m beam diameter, which could probably not be afforded or built. Cost is the penalty for using low C_m, high I_{sp} ablators. The per-unit-mass energy cost for delivery to LEO in column 3 is 13 times higher than in column 2, as predicted by figure 7. Note the even greater penalty paid for very high C_m values in figure 7.

We have assumed aerodynamic windows for the laser. Alternative beam diameters and thermal blooming gains are shown in column 3 for the reduced fluence required for solid-dielectric laser windows (such as CaF_2). Examples of the computer output for the thermal blooming instability calculations that appear in table 6 are shown in figures 9 and 10.

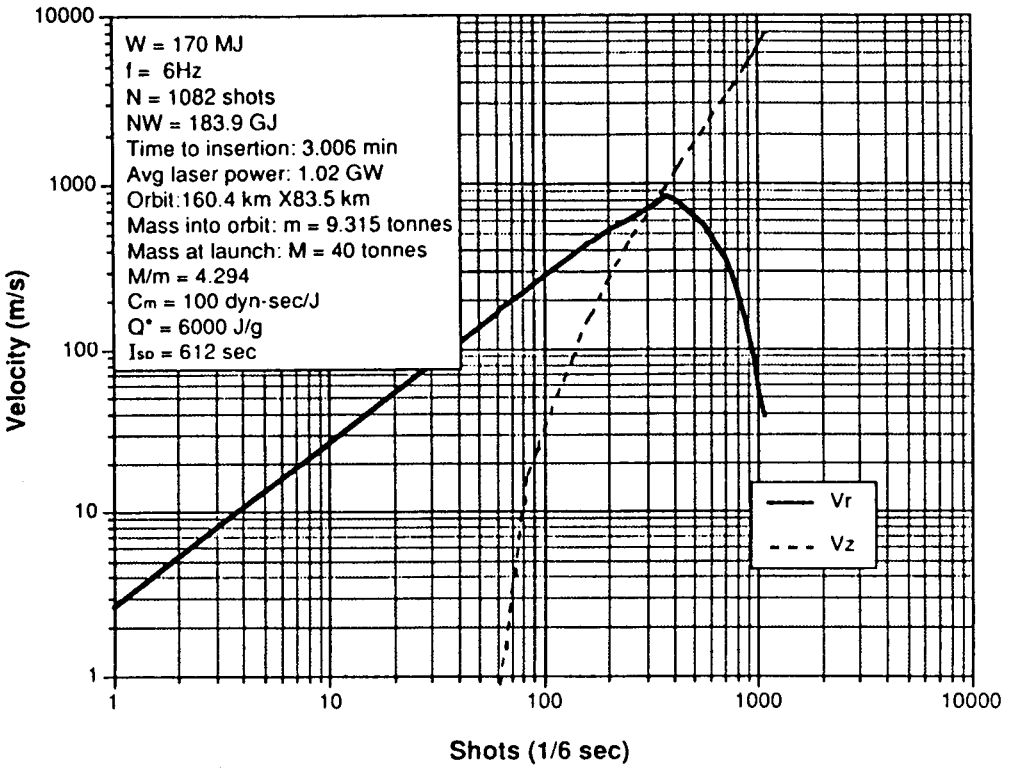

FIGURE 12. Calculated radial and down range velocity versus time.

6. Other LISP applications

We have studied other applications, and brief reports have been presented on these topics, including LEO-to-GEO transfer ("LEGO-LISP"), LEO reboost ("LO-LISP"), and deflection of near earth objects ("NEO-LISP"). We found that each application has a unique optimum coupling coefficient and laser parameters that are suited to the mission's economic factors. We will report this work in full detail in a future publication. Here, we will confine ourselves to briefly discussing geosynchronous satellite station keeping ("LISK"), which is the most attractive and lowest-cost near-term LISP application.

6.1. *Choice of wavelength and optical apertures for LISK*

LISK differs considerably from LISP because of the hundredfold increase in range. Laser wavelength λ is an important parameter determining range, since cost limits the diameter D_1 of the laser beam director when the ablation target and the laser source are widely separated. For propagation of a laser beam that is "μ times diffraction limited," the propagation theory as discussed in Section 4.1 gives for the range of the so-called beam waist:

$$z_R = \pi D_1^2/8\mu\lambda \quad \text{cm}. \tag{22}$$

An order of magnitude reduction in laser wavelength leads to an order of magnitude increase in range.

TABLE 8. Parameters for geosynchronous station keeping

Satellite angular correction	0.2 degrees
Interval	3 months
Satellite mass	3 tonnes
Δv	1.87 cm/s
δJ	$3.74 * 10^6$ dyne * s
C_m	100 dyne * s/J
Total laser energy $NW = N\Phi A$	37.4 kJ
Target intensity I	1 GW/cm^2
Target coupling area A	10 cm^2
Peak laser power P_{pk}	10 GW
Pulse duration τ	10 ns
Pulse energy W	100 J
Pulse repetition rate f	1 Hz
Total number of pulses N	374
Time to deliver correction	6.2 min
Average laser power P_{ave}	100 W
Laser wavelength	530 nm
Launch mirror diameter	3 m
Receiving mirror diameter	30 m
Beam quality μ	2.8
Mass ablated per 3-month correction	$(18.7/\eta_{AB})$g
Range	36,000 km

In the case of LISK, it is sensible to place a large receiving mirror of diameter D_2 on the satellite that focuses the received beam onto the ablation disk. The mirror can be low-quality aluminized mylar, since it will receive low fluence and its focusing requirements are not stringent. Then, the range z is dramatically increased:

$$z/z_R = 1 + [2(D_2/D_1)^2 - 1]^{1/2}. \tag{23}$$

6.2. *LISK system parameters*

Since $z = 36.000$ km for LISK, and we would like to use standard, observatory-type mirrors for the beam director ($D_1 = 3$ m), equations (22) and (23) show that, assuming $\mu = 2.8$, even with a relatively large receiving mirror ($D_2 = 30$ m), we are forced to use short wavelengths $\lambda \leq 530$ nm. In contrast, infrared gas lasers are most desirable for LEO-LISP because the shorter range permits them and they have low cost per joule.

We assume a geosynchronous satellite mass of 2 tonnes and a required positional drift correction of 0.2^0 per 3 months. The resulting velocity increment $\Delta v = 1.87$ cm/s can be provided with a coupling coefficient of $C_m = 100$ dyne s/J with a total laser energy of 37 kJ. The upper limit of target intensity required to generate this coupling coefficient is $I = 1$ GW/cm^2, and we take the focal spot area of the satellite's 30-m-diameter receiving mirror to be $A = 10$ cm^2, so a 10-GW laser pulse is required. With $D_1 = 3$ m, intensity in the atmosphere is 140 kW/cm^2. Because the beam will be generated by frequency doubling a 1.06-μm Nd:glass laser, we pick $\tau = 10$ ns pulse duration to simplify the doubling process, and the laser energy is W = 100 J per pulse.

Then, the 37 kJ to reposition the satellite will require a total of $N = 370$ pulses, which, at 1 Hz, can be applied over 6.2 min. The average laser output power is just 100 W. The mass ablated per 3-month correction is just $1.87/\eta_{AB}$ g, giving a lifetime of 100 years for a 10-kg ablation disk under ideal conditions. Considering the cost of geosynchronous sat-

ellites, and the fact that one laser can obviously keep a number of satellites properly positioned, this is a very attractive case for immediate application.

Such a laser could be built easily and cheaply [probably < \$100k] using standard components developed for ICF. The most expensive components of the system would be the beam director and tracking system, but these would certainly not be dedicated to LISK and could be used most of the time for more conventional purposes. The geosynchronous satellite would require extra design features to receive and utilize the laser pulse. These consist of a large receiving optic, an ablator, and a rudimentary pointing mechanism to direct ablator thrust. The optics would be a self-deploying aluminized mylar sheet supported by a lightweight structure. It might be easiest to make the sheet in planar form with embossed grooves to form a reflective analog to a Fresnel lens. We estimate the total cost of the laser system and modifications for one geosynchronous satellite to be \$1M. The cost of a single geosynchronous satellite is on the order of \$250M, but its lifetime is limited to about 10 years by dissipation of station keeping fuel. Granting the conservative assumption that we can extend this lifetime using LISK by a factor of 5 indicates that the benefit-to-cost ratio of a LISK setup is 1000:1 at a minimum.

Laser intensity incident on the receiving optic is just 1.4 kW/cm^2 (fluence 14 μJ/cm^2), so there is no danger of optical damage. If the focal length of the mirror is equal to its diameter, its required optical quality is 1.2 mrad, a performance that is readily achieved by the types of receiving optics suggested.

7. Outline for further research, near-term applications, and futuristic concepts

Following on Kantrowitz' question, one might ask what research should be undertaken in the immediate future and with what near-term application in mind? How can newcomers to this exciting field become involved? We believe this can best be answered by an immediate expansion in LISP research, financed by government and industry made aware of short-term applications such as LISK.

7.1. *Future research*

Before LEO-LISP can seriously be envisaged, a number of scientific and engineering objectives need to be achieved. These objectives are a convincing demonstration of a high-power DF laser and of the delivery optics.

The laser fusion and X-ray laser programs have taught the lesson that orders of magnitude extrapolation of power, though achievable, always introduce unforeseen problems. Seemingly straightforward laser experiments such as the Beat Wave Accelerator turn out nigh impossible. Some potential engineering problems with a high-power, long-pulse, high-repetition rate DF laser are as follows:

Gasdynamic: Care in design must be taken to avoid turbulence.

Initiation: Can efficient photoinitiation avoid some of the problems with large-size electron guns?

Delivery optics: "Active optics" mirrors hold great promise, but to our knowledge no one has yet operated such a mirror in conjunction with a very high power, "rep rated" laser system. With LISK the problem may be less severe than for LISP, but kilowatts (let alone megawatts) of cooling in an active mirror will introduce engineering complexities.

Coupling coefficient: It is necessary to develop and demonstrate examples of high and moderate C_m that occur together with high ablation efficiency η_{AB} for laser wavelengths

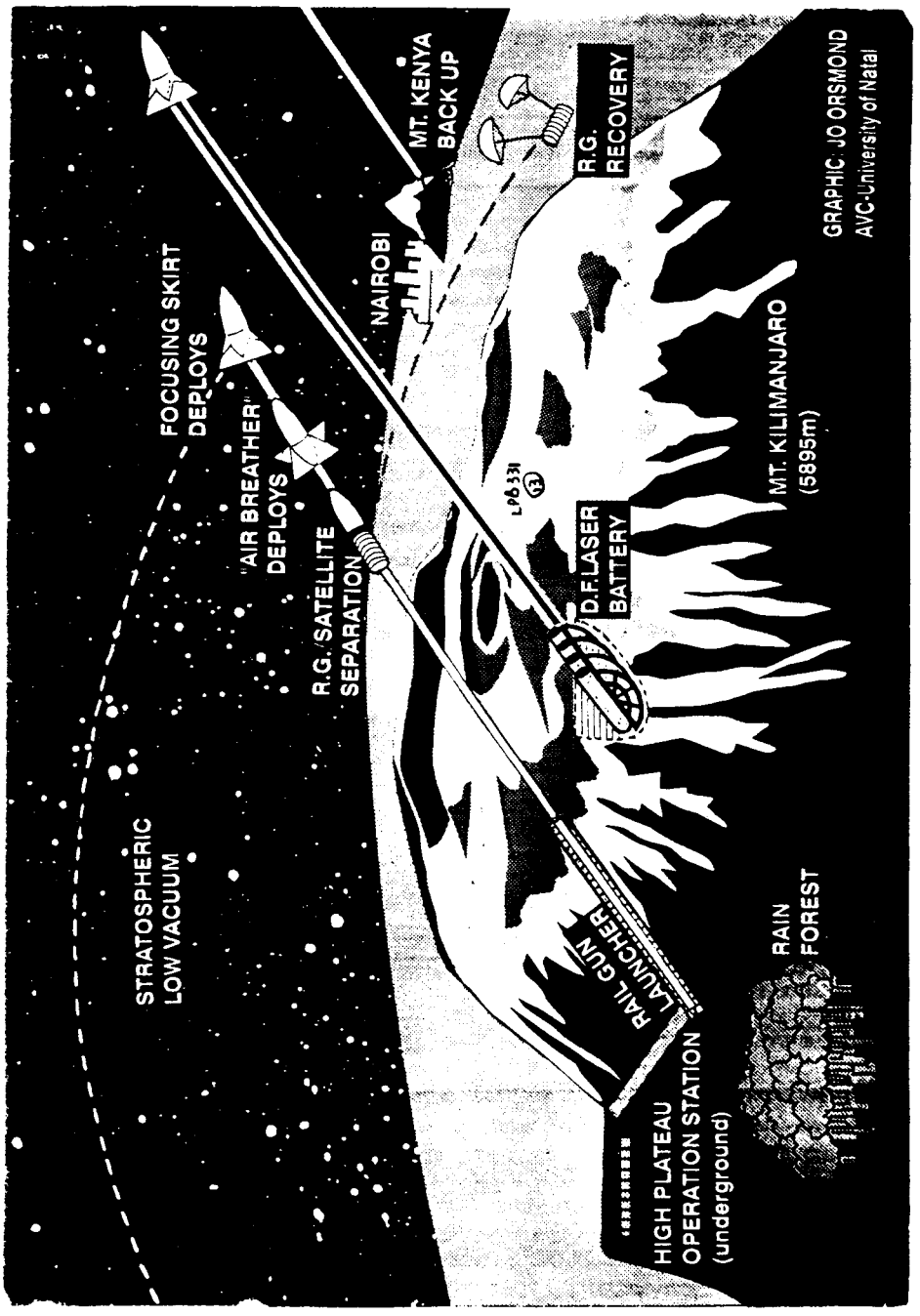

FIGURE 13. Futuristic HSP concept.

from the ultraviolet through the visible to the near infrared. These may be stratified target structures, but they must be cheap to manufacture in large quantities.

In order to persuade the financial and political world that LISP is viable, we suggest a proof of principle experiment on a much smaller scale but similar in spirit to the TFTR and JET experiments that did so much for fusion funding. The most practical near-term program is the development of a LISK system and its practical demonstration, first in the laboratory and then in space. Such a program would be a good testbed for programs that still exist with high-speed active mirrors, development of large lightweight spaceborne collection optics, and for demonstration of large vacuum coupling coefficients in the visible.

7.2. *Futuristic concepts*

The power of futuristic concepts to influence should not be underestimated. One exciting concept is that of an equatorial world laser launch center. One of the furthest points from the earth's center is Uhuru on the edge of the dormant Kilimanjaro crater (farther than Everest and K1 but not Ecuador's active volcano Chimborazo). One might imagine a hybrid launch system consisting of a subterranean vacuum rail gun and a battery of DF lasers. (The ecological impact of the system could be minimized by insisting that the lasers also be below the surface and all exit holes inside the crater.) The ecological advantages of such a laser launch center would need to be investigated. Whilst solid booster rockets will release ever greater amounts of chlorine and nitrous oxides into the stratosphere, it would seem at first glance very advantageous to reduce the "fuel" mass by an order of magnitude. But if the fuel itself contains ozone destroying catalysts or potent greenhouse compounds, the ecological gain may be nil. However, the flexibility exists with laser ablation of deliberately designing the ablation material to mitigate the ozone problem by releasing compounds that bind monatomic chlorine or actually release monatomic oxygen. It would also be important to investigate the question of "sound pollution." Laser launches will be very noisy indeed (Kare 1987) but perhaps no more so than a powerful equatorial storm. In concluding this section we present an artist's impression of an equatorial laser launch center and a sketch of the gigawatt laser battery needed to launch a 5-tonne satellite. The satellite is equipped with a small laser that beams a signal down to ground via a pod supported mirror. The mirror position is continuously adjusted so that the return beam impacts the rear of the satellite precisely. The ground lasers are mounted on a hydraulically supported platform and track the satellite continuously. Fine tracking is obtained from an active optics system (AOS) that uses the small satellite signal to direct a powerful return beam. The wave front of this conjugate beam is thus profiled to come to a focus exactly where the satellite mirror was. It is also conceivable that pulsed gas lenses may be used to focus the beams in and out of the AOS. Gas lenses have been shown to have good optical qualities (Michaelis *et al.* 1991).

8. Conclusion

Laser propulsion, with or without the high-power laser fusion community, will doubtless become reality. With cooperation, one might even see a laser impulse station keeping (LISK) experiment this century and the first laser launch early in the next.

Acknowledgments

The authors are grateful for useful discussions of the LEO-to-GEO transfer problem with Dr. Gene McCall of Los Alamos National Laboratory, and to Dr. David Rosen of Physi-

cal Sciences, Inc., Andover, Massachussets, USA, for the use of their 10.6-μm laser facility in obtaining our pyroxilin data, and for the generous permission to quote their own data on glass at 10.6 μm. We also thank Jo Orsmond and Arnold Prause for technical help and advice with the paper.

REFERENCES

ACTON, D.S. & SMITHSON, R.C. 1989 In *Proceedings of the Tenth Sacramento Peak Summer Workshop on High Spatial Resolution Solar Observations*, O. von der Luhe, ed.

ASHOOR, R. *et al.* 1989 Euromech 257 Conf. Marseille.

BARNARD, J.J. 1989 *Appl. Opt.* **28**, 438.

CHAPMAN, P.K. *et al.* 1977 AVCO-EVERETT, DARPA Order 3138.

ESHBACH, O.W. 1952 *Handbook of Engineering Fundamentals*, 2nd ed. (John Wiley, New York), p. 8.

FABBRO, R. *et al.* 1991 *J. Appl. Phys.* **68**, 775.

KANTROWITZ, A. 1972 *Astronaut. Aeronaut.* **10**, 74.

KANTROWITZ, A. 1986 *Proc. SDIO/DARPA Workshop on Laser Propulsion*, J.T. Kare, ed. LLNL Conf-860778, **2**, Livermore, CA, 1987, p. 1.

KARE, J.T. 1987 In *Proc. SDIO/DARPA Workshop on Laser Propulsion*, LLNL Conf-8710452, Livermore, CA, 1990.

KARE, J.T. 1989 In *Current Topics in Shockwaves* Y.W. Kim, ed., AIP Conference Proceedings 208, American Institute of Physics 1990, p. 359.

KELLY, R. & DREYFUS, R.W. 1988 *Nucl. Inst. Meth.* **B32**, 341.

KOGELNIK, H. & LI, T. 1966 *Appl. Opt.* **5**, 1550.

MARX, G. 1966 *Nature* **211**, 22.

MEHTA, N.C. 1992 (private communication).

MICHAELIS, M.M. *et al.* 1991 *Nature* **353**, 547.

MOECKEL, W.E. 1972a *J. Spacecraft and Rockets* **9**, 863.

MOECKEL, W.E. 1972b *J. Spacecraft and Rockets* **9**, 942.

MOECKEL, W.E. 1975 *J. Spacecraft and Rockets* **12**, 700.

PHIPPS, C.R. 1989 *Laser and Particle Beams* **7**, 835.

PHIPPS, C.R. 1990 Los Alamos National Laboratory Report LA-11832-MS.

PHIPPS, C.R. 1992a In *Proceedings of the 9th International Symposium on Gas Flow and Chemical Lasers*, Elounda, Crete.

PHIPPS, C.R. 1992b In *Proceedings of the Near-Earth-Object Interception Workshop*, Report LA-12476-C, Los Alamos National Laboratory, Los Alamos, NM, USA.

PHIPPS, C.R. *et al.* 1988 *J. Appl. PHys.* **64**, 1083.

PHIPPS, C.R. *et al.* 1990 *Laser and Particle Beams* **8**, 281.

PHIPPS, C.R. & MICHAELIS, M.M. 1992 *Conference on Physics of Nuclear Induced Plasmas and Problems of Nuclear Pumped Lasers.* Obninsk, Russia.

PHIPPS, C.R. & DREYFUS, R.W. 1993 In *Laser Ionization Mass Analysis*, A.V. Renaat Gijbels & F. Adams, eds. (John Wiley, New York).

POTTER, J.H. 1967 *Handbook of Engineering Sciences II* (Van Nostrand, New York), p. 310.

RAIZER, YU.P. 1970 *Sov. Phys.–JETP* **31**, 1148.

SÄNGER, E. 1956 *Aero Digest* (UK), p. 68.

YORK, G.W. 1991 (private communication).

APPENDIX

Monoenergetic versus real velocity distributions

In the discussion of laser momentum coupling physics in Section 2, a simplifying assumption was made in order to make the relationships among variables more clear. This assump-

$$\psi = \frac{\langle v_x^2 \rangle}{(\langle v_x \rangle)^2} = \left\{ \frac{u^2 + \dfrac{kT}{m_E}}{u^2} \right\}. \tag{A10}$$

If, for example, we take the drift velocity equal to the soundspeed, $u = c_s = \sqrt{(\gamma kT/m_E)}$, then we find $\psi = (\gamma + 1)/\gamma = 1.60$.

However, when the angular distribution of particle density in a planar-target laser ablation plume in vacuum is investigated, a preponderance of measurements summarized in Kelly and Dreyfus (1988) and in Phipps and Dreyfus (1993) show forward peaking that is highly pronounced relative to the angular distribution predicted by equation (A1) with a sonic drift velocity $u = c_s$. Where θ is the angle to the surface normal, it is observed that the detected plume distribution varies like $\cos^{\nu}\theta$, with several experiments giving a beamlike expansion with $\nu = 8 - 10$. This beamlike behavior of real ablation jets, in which the half-width at half-maximum is of order 20 degrees, is the reason why we need not consider anything more complex than ablation from planar targets in this work. Nature forms the jet already.

Kelly and Dreyfus show that, introducing the drift velocity Mach number $\mathcal{M} = u/c_s$, $\mathcal{M} = 1$ should correspond to $\nu = 4$, whereas $\nu = 8 - 10$ corresponds to $\mathcal{M} \approx 2$. In other words, the flow in high-intensity laser ablation is supersonic. This rather strange result has two possible causes whose relative importance has not yet been assessed. These are 1) acceleration of the stream due to unsteady adiabatic expansion beyond the Knudsen layer as discussed by Kelly and Dreyfus (1988), and 2) electrostatic acceleration of the ions in the plasma stream by the collisionally decoupled high-energy tail of the electron velocity distribution as discussed by Phipps and Dreyfus (1993). When $\mathcal{M} = 2$,

$$\psi = \frac{4\gamma + 1}{4\gamma} = 1.15. \tag{A11}$$

In the above we have taken the specific heat ratio $\gamma = c_p/c_v = 5/3$ (the ideal gas value), which is valid for the typical LISP laser-ablation plume. In fact, the assumptions made in writing equation (7) of the text are fairly good. Note that

$$\eta_{AB} = \frac{\delta m \langle v_E^2 \rangle}{2 \times 10^7 \Phi} \geq \frac{\delta m \langle v_E \rangle^2}{2 \times 10^7 \Phi} \quad \text{overestimates } \eta_{AB}.$$

tion, stated following equation (5), is that the exhaust velocity distribution is to be considered monoenergetic for analytical simplicity. Where by $\langle v_x^m \rangle$ we mean the mth moment of v_x, this statement allows us to take $\langle v_x^2 \rangle = (\langle v_x \rangle)^2$, a result that would give very misleading results in some circumstances. While it is clear that subsequent mathematics [e.g., equation (10a)] will become highly opaque if we carry along the velocity-space integrals that make the analysis rigorous, we need to analyze the error implicit in doing so for a real exhaust stream, to justify the shorthand used in the main body of the paper.

We consider free expansion in the x-direction perpendicular to a planar target of the LISP type. After thermalization has taken place in the stream immediately adjacent to the thin so-called "Knudsen layer" at the laser-heated surface, the velocity distribution of the ablated particles is a full-range three-dimensional Maxwell–Boltzmann velocity distribution with drift velocity u in the x-direction (Kelly & Dreyfus 1988):

$$f(v_x, v_y, v_z) = C_x C_y C_z \{\exp - \beta[(v_x - u)^2 + v_y^2 + v_z^2]\}, \tag{A1}$$

where

$$\beta = \frac{m_E}{2kT} \qquad \text{and} \qquad C_i \ni \int_{-\infty}^{+\infty} dv_i f(v_i) = 1. \tag{A2}$$

That is,

$$C_x = C_y = C_z = \sqrt{\frac{\beta}{\pi}}. \tag{A3}$$

In equation (A2), m_E is the exhaust particle mass. The precise definition of impulse generated by one laser pulse is

$$\delta p = \delta m \langle v_x \rangle \tag{A4}$$

and

$$C_m = \frac{\delta m \langle v_x \rangle}{\Phi}. \tag{A5}$$

In the text, we use v_E to denote $\langle v_x \rangle$. With the equation (A1) velocity distribution,

$$\langle v_x \rangle = \int_{-\infty}^{+\infty} dv_x v_x f(v_x) = C_x \left[\sqrt{\frac{\pi}{\beta}}\, u \right] = u. \tag{A6}$$

The amount of kientic energy in the stream is

$$e = \tfrac{1}{2} \delta m \langle v_x^2 \rangle \tag{A7}$$

where

$$\langle v_x^2 \rangle = \int_{-\infty}^{+\infty} dv_x v_x^2 f(v_x) = C_x \left[\frac{\sqrt{\pi}}{2\beta^{3/2}} + \sqrt{\frac{\pi}{\beta}}\, u^2 \right] = \left[\frac{kT}{m_E} + u^2 \right]. \tag{A8}$$

Thc ablation efficiency η_{AB} is defined by

$$\eta_{AB} = \frac{e}{10^7 \Phi}. \tag{A9}$$

In the text, equation (7), we implicitly replace $\langle v_x^2 \rangle$ by $(\langle v_x \rangle)^2$ for analytical convenience. To gauge the consequence of this substitution, we calculate the ratio ψ from equations (A4) and (A8) and find:

$$\psi = \frac{\langle v_x^2 \rangle}{(\langle v_x \rangle)^2} = \left\{ \frac{u^2 + \dfrac{kT}{m_E}}{u^2} \right\}. \tag{A10}$$

If, for example, we take the drift velocity equal to the soundspeed, $u = c_s = \sqrt{(\gamma kT/m_E)}$, then we find $\psi = (\gamma + 1)/\gamma = 1.60$.

However, when the angular distribution of particle density in a planar-target laser ablation plume in vacuum is investigated, a preponderance of measurements summarized in Kelly and Dreyfus (1988) and in Phipps and Dreyfus (1993) show forward peaking that is highly pronounced relative to the angular distribution predicted by equation (A1) with a sonic drift velocity $u = c_s$. Where θ is the angle to the surface normal, it is observed that the detected plume distribution varies like $\cos^{\nu}\theta$, with several experiments giving a beamlike expansion with $\nu = 8 - 10$. This beamlike behavior of real ablation jets, in which the half-width at half-maximum is of order 20 degrees, is the reason why we need not consider anything more complex than ablation from planar targets in this work. Nature forms the jet already.

Kelly and Dreyfus show that, introducing the drift velocity Mach number $\mathcal{M} = u/c_s$, $\mathcal{M} = 1$ should correspond to $\nu = 4$, whereas $\nu = 8 - 10$ corresponds to $\mathcal{M} \approx 2$. In other words, the flow in high-intensity laser ablation is supersonic. This rather strange result has two possible causes whose relative importance has not yet been assessed. These are 1) acceleration of the stream due to unsteady adiabatic expansion beyond the Knudsen layer as discussed by Kelly and Dreyfus (1988), and 2) electrostatic acceleration of the ions in the plasma stream by the collisionally decoupled high-energy tail of the electron velocity distribution as discussed by Phipps and Dreyfus (1993). When $\mathcal{M} = 2$,

$$\psi = \frac{4\gamma + 1}{4\gamma} = 1.15. \tag{A11}$$

In the above we have taken the specific heat ratio $\gamma = c_p/c_v = 5/3$ (the ideal gas value), which is valid for the typical LISP laser-ablation plume. In fact, the assumptions made in writing equation (7) of the text are fairly good. Note that

$$\eta_{AB} = \frac{\delta m \langle v_E^2 \rangle}{2 \times 10^7 \Phi} \geq \frac{\delta m \langle v_E \rangle^2}{2 \times 10^7 \Phi} \quad \text{overestimates } \eta_{AB}.$$